Hydraulics of Closed Conduit Spillways

Part XVI:
Elbows and Transitions for the Two-Way Drop Inlet

Advances in Agricultural Technology
Science and Education Administration
U.S. Department of Agriculture

AAT-NC-1
February 1979

ERRATA

Hydraulic Model Investigation of a Two-Way Drop Inlet
For Floodwater Retarding Structure No. 3
Banklick Creek Watershed,
Boone and Kenton Counties, Kentucky
ARS-NC-63, August 1978

In Figure 13 as shown below:

"Figure 14" should read "Figure 14,A"

"Figure 15" should read "Figure 14,B"

"Figure 16" should read "Figure 15,A"

"Figure 17" should read "Figure 15,C"

"Figure 18" should read "Figure 15,B"

"Figure 19" should read "Figure 16"

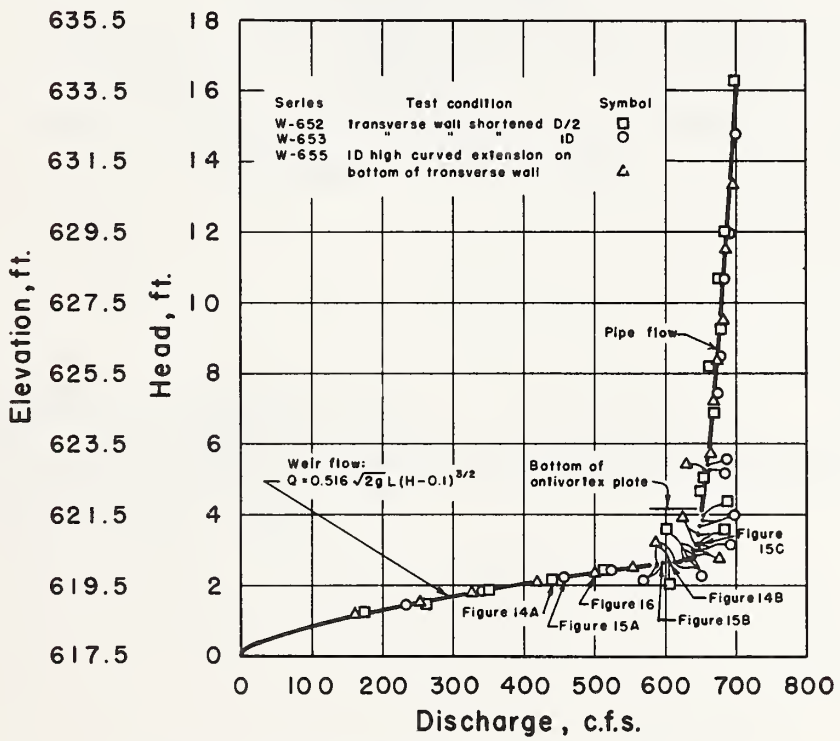

Figure 13.—Model head-discharge relationships with transverse splitter wall modifications.

Editor's note: Paste corrected chart in place on page 11.

GPO 821-991

Study conducted by
Agricultural Research
Science and Education Administration
UNITED STATES DEPARTMENT OF AGRICULTURE
in cooperation with
Minnesota Agricultural Experiment Station
and the
St. Anthony Falls Hydraulic Laboratory
University of Minnesota

This publication is available from the
St. Anthony Falls Hydraulic Laboratory, Agricultural Research
Science and Education Administration, U.S. Department of Agriculture
Third Ave. SE at Mississippi River
Minneapolis, Minn. 55414.

Other publications in this series are discussed in the Preface.

Published by Agricultural Research (North Central Region),
Science and Education Administration, U.S. Department of Agriculture, Peoria, Ill. 61614.

PREFACE

This publication, the 16th part of a group of publications dealing with the hydraulics of closed conduit spillways, reports tests on the elbow and transition used between high two-way drop inlets and the spillway barrel. The previous 15 parts were published as technical papers and Agricultural Research Service (ARS-NC Series) publications all under the major title "Hydraulics of Closed Conduit Spillways." The technical papers were published by the St. Anthony Falls Hydraulic Laboratory (SAFHL), University of Minnesota, Minneapolis. The earlier publications are:

Part I. Theory and Its Application, by F. W. Blaisdell. SAFHL Tech. Paper No. 12, Ser. B, 22 pp., illus., Jan. 1952 (rev. Feb. 1958). Gives theory, symbols, and bibliography.

Parts II through VII. Results of Tests on Several Forms of the Spillway, by F. W. Blaisdell. SAFHL Tech. Paper No. 18, Ser. B, 50 pp., illus., March 1958. Parts II through VI describe the hydraulic performance and present discharge coefficients for five forms of the closed conduit spillway; Part VII discusses vortices and their effect on the spillway capacity.

Part VIII. Miscellaneous Laboratory Tests; Part IX. Field Tests, F. W. Blaisdell. SAFHL Tech. Paper No. 19, Ser. B, 54 pp., illus., March 1958. Reports tests on models of specific field structures and on field structures themselves.

Part X. The Hood Inlet, F. W. Blaisdell and C. A. Donnelly. SAFHL Tech. Paper No. 20, Ser. B, 41 pp., illus., April 1958. Reports the development of the hood inlet.

Part XI. Tests Using Air, F. W. Blaisdell and G. G. Hebaus. SAFHL Tech. Paper No. 44, Ser. B, 53 pp., illus., January 1966. Discusses the use of air for tests of closed conduit spillways.

Part XII. The Two-Way Drop Inlet with a Flat Bottom, C. A. Donnelly, G. G. Hebaus, and F. W. Blaisdell. ARS-NC-14, 66 pp., illus., September 1974. Discusses tests on a covered rectangular drop inlet with a flat bottom where the water enters only over the two sides, and presents recommendations for the spillway design.

Part XIII. The Hood Drop Inlet, K. Yalamanchili and F. W. Blaisdell. ARS-NC-23, 78 pp., illus., August 1975. Reports tests on a hood inlet located at the bottom of a drop inlet and gives recommendations for its proportioning and hydraulic design.

Part XIV. Antivortex Walls for Drop Inlets; Part XV. Low-Stage Inlet for the Two-Way Drop Inlet, C. A. Donnelly and F. W. Blaisdell. ARS-NC-33, 37 pp., illus., March 1976. Part XIV reports tests on the adequacy of various antivortex devices for square, rectangular, and circular drop inlets. Part XV reports tests on the location and size of low-stage orifices for two-stage, two-way drop inlets.

The elbow and transition study reported in this publication, Part XVI, was conducted by engineers of Agricultural Research, Science and Education Administration, U. S. Department of Agriculture, Minneapolis, cooperating with the Minnesota Agricultural Experiment Station and the St. Anthony Falls Hydraulic Laboratory, University of Minnesota, Minneapolis. George G. Hebaus conducted the preliminary literature search, developed the experimental program, and conceived the unique form of the warped transition. Charles E. Rice designed the air models and conducted most of the air tests. Clayton L. Anderson completed the air experiments, designed the water models, conducted the water tests, analyzed the data, and wrote the report. Charles A. Donnelly assisted with the water tests. The entire study was completed under the direction of Fred W. Blaisdell, research leader and technical advisor for structures for water control and measurement.

CONTENTS

Hydraulics of Closed Conduit Spillways

Part XVI:
Elbows and Transitions for the Two-Way Drop Inlet

Clayton L. Anderson[1]

INTRODUCTION

The possibility of cavitation damage occurring in tall closed conduit spillways has been recognized for many years. For drop inlet spillway entrances, a likely place for cavitation damage to occur is in the barrel just downstream from the drop inlet. The objective of this study is to develop and evaluate a cavitation-free elbow between the drop inlet and a transition, and a cavitation-free transition between the square cross section at the elbow exit and a circular barrel.

For short drop inlets the barrel entrance is frequently square-edged because it is the most economical to use, the greater entrance energy loss can be readily tolerated, and the velocities are low so cavitation will not occur. However, for sufficiently tall drop inlets, cavitation damage can be anticipated if the simple square-edged barrel entrance is used. Thus, for tall drop inlets there is need for a barrel entrance that will reduce the possibility of cavitation and the subsequent damage to the conduit caused by the collapse of the cavitation bubbles on the conduit wall.

The two-way drop inlet reported in Part XII[2,3] is widely used by the Soil Conservation Service (SCS) in its watershed protection and flood prevention, resource conservation and development, and other water resource programs. Many of these two-way drop inlets are so tall that cavitation damage is possible if the square-edged barrel entrance presented in Part XII is used. The study reported herein is a result of the need for cavitation-free or low cavitation potential barrel entrances for the two-way drop inlet.

As a result of this study, two elbow shapes, elbows 3 and 6, and two transition shapes, transitions A and F, all described in the section ELBOWS AND TRANSITIONS TESTED, are recommended.

PREVIOUS WORK

An elbow and transition for a two-way drop inlet was tested for the SCS at Swarthmore College,[4] Swarthmore, Pa. The Swarthmore study was conducted on a 1/15 scale model of the drop inlet shown in figure XVI-1. A transition section was required to transform the 2 ft (0.61 m) wide by 4 ft (1.22 m) high (1**D** × 2**D**) (**D** = barrel diameter) rectangular cross section B-B to the 2 ft (0.61 m) (1**D**) diameter circular cross section A-A of the conduit. The corners of

---

[1] Hydraulic engineer, St. Anthony Falls Hydraulic Laboratory, Agricultural Research, Science and Education Administration, U.S. Department of Agriculture, Third Ave. SE at Mississippi River, Minneapolis, Minn. 55414.

[2] The Roman numerals in references to equations, figures, and parts refer to a particular part of this report series cited in the Preface.

[3] The two-way drop inlet reported in Part XII has a flat bottom and is used by SCS for square and rectangular barrels. When the barrel is circular, SCS uses a horizontal semicylinder of **D**/2 radius as the bottom of the drop inlet. Results of tests on the semicylindrical bottom drop inlet will be reported in Part XVII.

[4] Willis, M. J. and Newlin, C. W. Report on Hydraulic Testing of Scale Model of Drop Spillway for Grave Creek Project, Civil Engineering Department, Swarthmore College, Swarthmore, Pa. 1958.

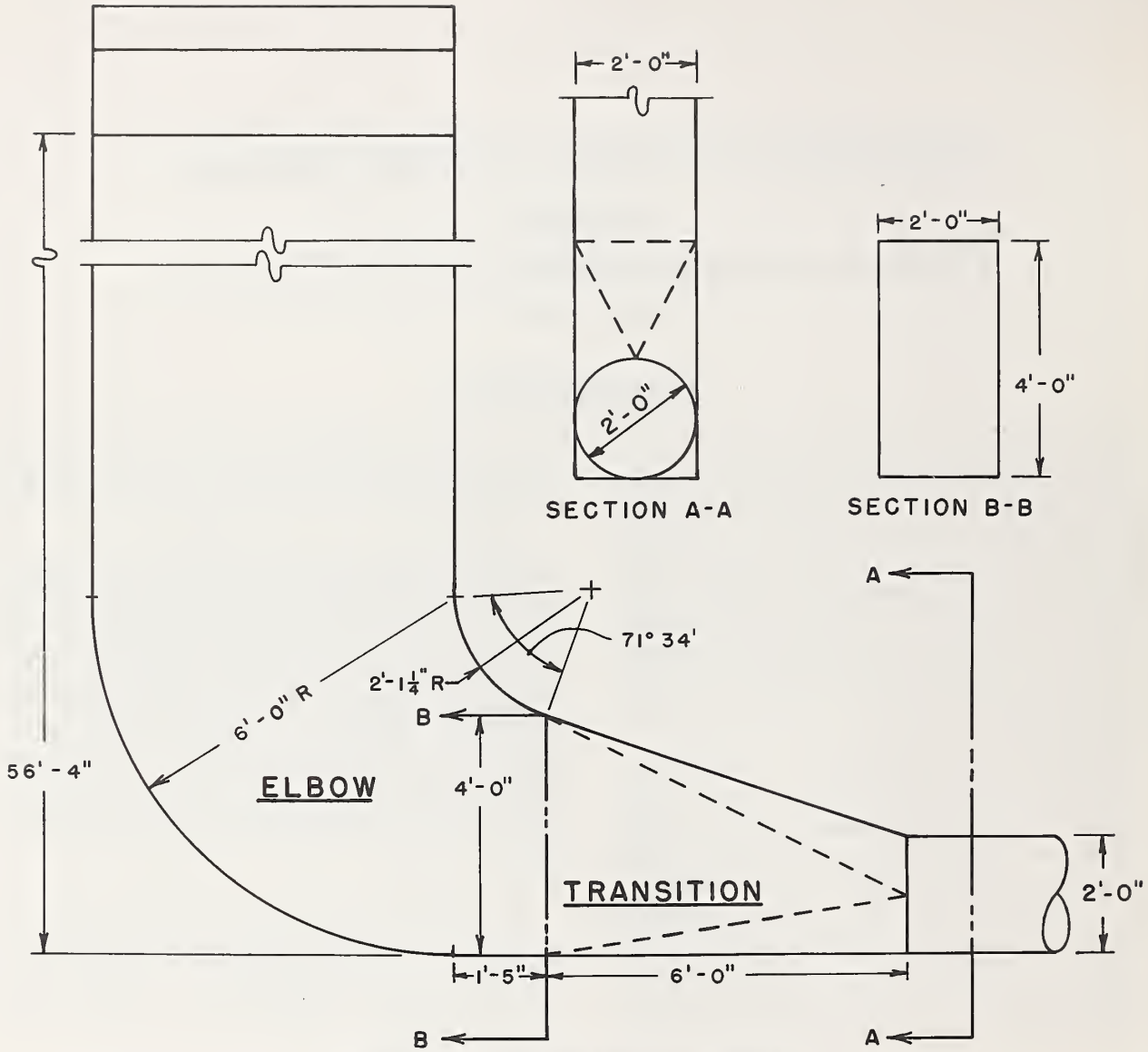

Figure XVI-1.—Swarthmore elbow and transition.

the transition section were quarter conical surfaces. The sidewalls, top, and bottom of the transition were plane triangular surfaces.

The Swarthmore elbow and transition was also tested at the U.S. Army Engineer Waterways Experiment Station.[5]

ELBOWS AND TRANSITIONS TESTED

Six elbows (Nos. 1 through 6) and seven transitions (A through G) were tested. Before describing the elbows and transitions, the primary considerations involved in their selection will be explained.

Practical Considerations

Because the Swarthmore elbow and transition were difficult to form, SCS Engineering Division engineers suggested that the steeply sloping top of the transition be flattened to be an extension of the barrel slope. This requires

[5] Grace, Jr., J. L. Outlet Works for Branched Oak and Cottonwood Springs Dams, Oak Creek, Nebr., and Cottonwood Springs Creek, S.D., U.S. Army Engineer Waterways Experiment Station, Vicksburg, Miss., Technical Report H-72-1, January 1972. 30 pp.

TABLE XVI-1.—*Elbows tested*

Elbow	Shape	Curvature	Barrel slope	Length	Height
1	Ellipse	3D/2 × D/2	0.000	1.50D	0.50D
2	Ellipse	5D/4 × 3D/4	.000	1.25D	.75D
3	Ellipse	2D × D	.000	2.00D	1.00D
4	Free streamline	equations XVI-1	.025	2.35D	.86D
5	Double circle	45° @ r = D/2, 45° @ r = D	.000	.85D	.65D
6	Double circle	45° @ r = D/2, 45° @ r = 3D/2	.000	1.21D	.79D

that the downstream end of the elbow be tangent to the barrel crown. The upstream end of the elbow is tangent to the downstream endwall of the drop inlet. For simplicity of construction, the elbow should be a surface of single curvature. The SCS engineers also suggested that, for barrel velocities less than 30 ft/s (9.1 m/s), the elbow be composed of circular segments of D/2 radius for 45° and D radius for the remainder of the elbow. This is elbow 5 (see table XVI-1, above). For barrel velocities exceeding 30 ft/s (9.1 m/s), an elliptical elbow developed by the U.S. Army Corps of Engineers was suggested. This is elbow 1. For the transition, SCS engineers suggested triangular planes and quarter conical surfaces. This is transition A (see table XVI-2, page 4).

If the barrel is circular, current SCS practice is to make the bottom of the drop inlet a horizontal semicylinder of radius D/2. Extension of the semicylindrical invert through the elbow and transition means that only the upper half of the conduit must be transformed from semirectangular at the elbow exit to semicircular at the barrel entrance. If the barrel cross section is rectangular, the bottom of the drop inlet is flat, the cross section in the elbow is rectangular, and no transition is required. These are the invert shapes for the circular and square barrel shapes used in this study. The crown shapes were varied as described in the following sections.

Elbows

The six elbows tested are listed in table XVI-1.

Elbow 1 is conduit entrance shape D tested and suggested by the Corps of Engineers.[6] It has more cavitation potential than elliptical shape C (2D × 2D/3) and compound elliptical shape H—the best of the entrances tested by the Waterways Experiment Station.

The elbow 2 shape was selected as the best of the sluice gate lip profiles studied by Mueller.[7]

Elbow 3 has less curvature than elbows 1 and 2. This elbow shape was tested because the pressures along elbows 1 and 2 were lower—and therefore exhibited greater cavitation potential—than was felt desirable.

Elbow 4 was defined by the free streamline profile obtained from the potential flow development by Michell.[8]

The free streamline is considered a desirable elbow profile because pressure is constant along the free streamline and the tendency for flow separation is avoided. However, the pressure may not be constant when a fixed boundary replaces the free streamline. Although use of this profile may not be practical because of its great length, the results obtained with the free streamline elbow profile provide a basis for comparison with the other profiles tested.

The equations for the free streamline profile, as corrected by George G. Hebaus[9] and modified to express the coordinates in terms of the pipe diameter, are:

[6] Murphy, T. E. Investigation of Entrances Flared in Three Directions and In One Direction, U.S. Army Engineer Waterways Experiment Station, Vicksburg, Miss., Technical Memorandum No. 2-428, Report 2, June 1959, 13 pp., 15 tables, 21 plates.

[7] Rouse, H. Engineering Hydraulics. New York, John Wiley & Sons, Inc., 1950, p. 539.

[8] Michell, J. H. On the Theory of Free Streamlines. Philosophical Transactions of the Royal Society of London, Series A, MDCCCXC, Vol. 181, pp. 389-432.

[9] Research hydraulic engineer, St. Anthony Falls Hydraulic Laboratory, Agricultural Research, Science and Education Administration, U.S. Department of Agriculture, Third Ave. SE at Mississippi River, Minneapolis, Minn. 55414.

$$\frac{x}{D} = \frac{1}{\pi}\left\{\ln\frac{1-\cos\phi}{1+\cos\phi} + 2\left(\frac{a}{1-a}\right)^{1/2}\tan^{-1}\left[(\cos\phi)\left(\frac{1-a}{a}\right)^{1/2}\right]\right\}$$

$$\frac{y}{D} = -\frac{1}{\pi(1-a)^{1/2}}\ln\frac{1-(1-a)^{1/2}\sin\phi}{1+(1-a)^{1/2}\sin\phi} \qquad \text{(XVI-1)}$$

where the parameter **a** is a function of the drop inlet length **B**,

$$a = \left[\frac{(B/D)^2-1}{(B/D)^2+1}\right]^2,$$

and ϕ is the obtuse angle between the horizontal and the tangent to the free streamline. The limits are $0 \le a \le 1$, $\pi/2 \le \phi < \pi$, and in practice $1 \le B/D \le \infty$.

The shape of the free streamline profile was determined and constructed for a **B/D** ratio of 2. However, this profile was tested with various drop inlet lengths.

The origin of the coordinates is in the downstream face of the drop inlet at a distance **D** above the bottom of the drop inlet. The profile approaches the horizontal asymptotically at $x = \infty$ so, to limit the elbow length, the elbow profile was terminated at the point where the profile slope was 2.5 percent. A barrel slope of 2.5 percent was used for all tests with elbow 4.

Elbow 5 was that proposed by SCS.

Elbow 6 is similar to elbow 5, but the radius of the second arc was increased to 3**D**/2.

The rate of change of elbow curvature affects the ability of the flow to follow the elbow boundary. The elbow profiles are compared in figure XVI-2.

Transitions

The seven transitions tested are listed in table XVI-2 and the forms of the transitions are shown in figures XVI-3 and XVI-4.

Transition A has the form and dimensions suggested by SCS: triangular planes, quarter cones, and a length of 2**D**.

Transition B is similar to transition A except that its length is 1**D**.

The warped transition was developed from an idea originated by Hebaus.[10] This transition transformed the upper half of the elbow exit

[10] See footnote 9.

TABLE XVI-2.—*Transitions tested*

Transition	Length	Corners
A	2**D**	Conical, figure XVI-3
B	1**D**	Conical, figure XVI-3
C	1**D**	Warped, figure XVI-4 (a)
D	1**D**	Warped, figure XVI-4 (b)
E	1**D**	Warped, figure XVI-4 (c)
F	1**D**	Warped, figure XVI-4 (d)
G	**D**/2	Warped, figure XVI-4 (e)

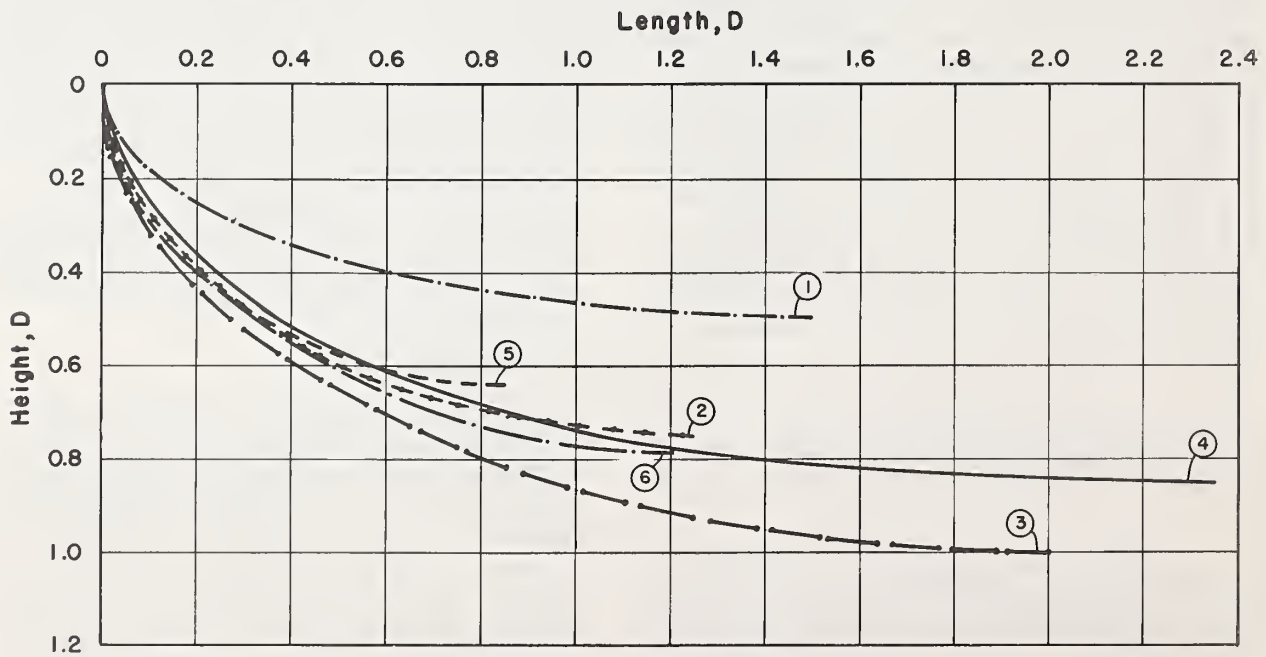

Figure XVI-2.—Elbow profiles.

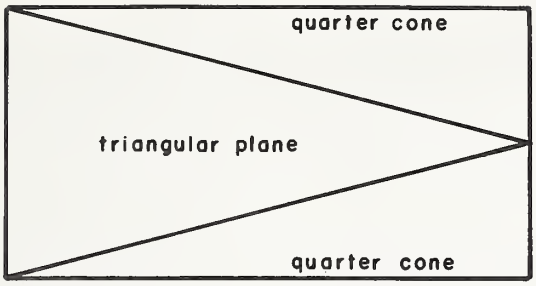

Top View

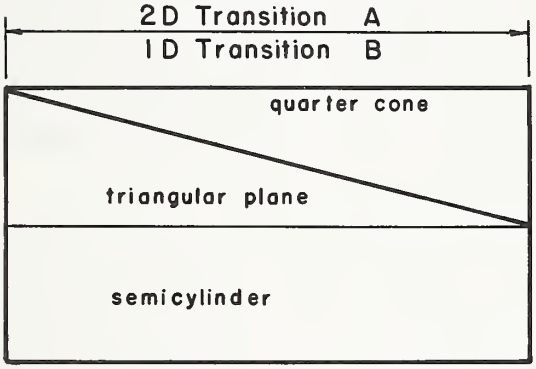

Side View

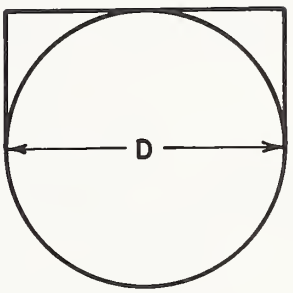

End View

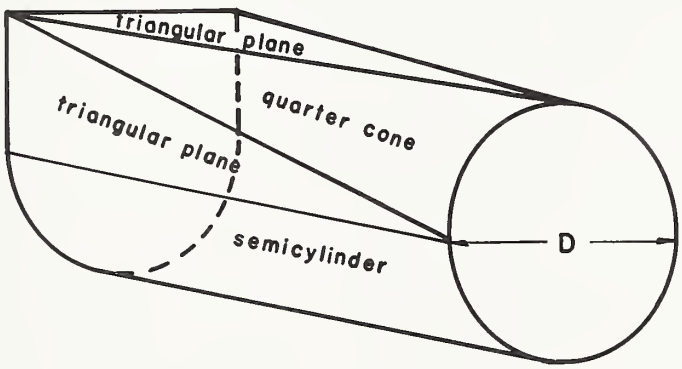

Oblique Projection

Figure XVI-3.—Conical transition geometry.

cross section with various forms of warped surfaces between a plane, horizontal top and the cylindrical portion of the transition section.

Two methods of defining the warped surfaces were developed.

For the first method, the transition section was defined by cutting the top half of the barrel to a given profile, as viewed from the side, beginning at D/2 above the invert at the entrance and ending at the crown at the downstream end of the transition. The equations for the profiles are shown in figures XVI-4(a)-(c). Successive tangents from the edge of the cut, normal to the barrel axis, to the horizontal plane through the barrel crown formed the warped

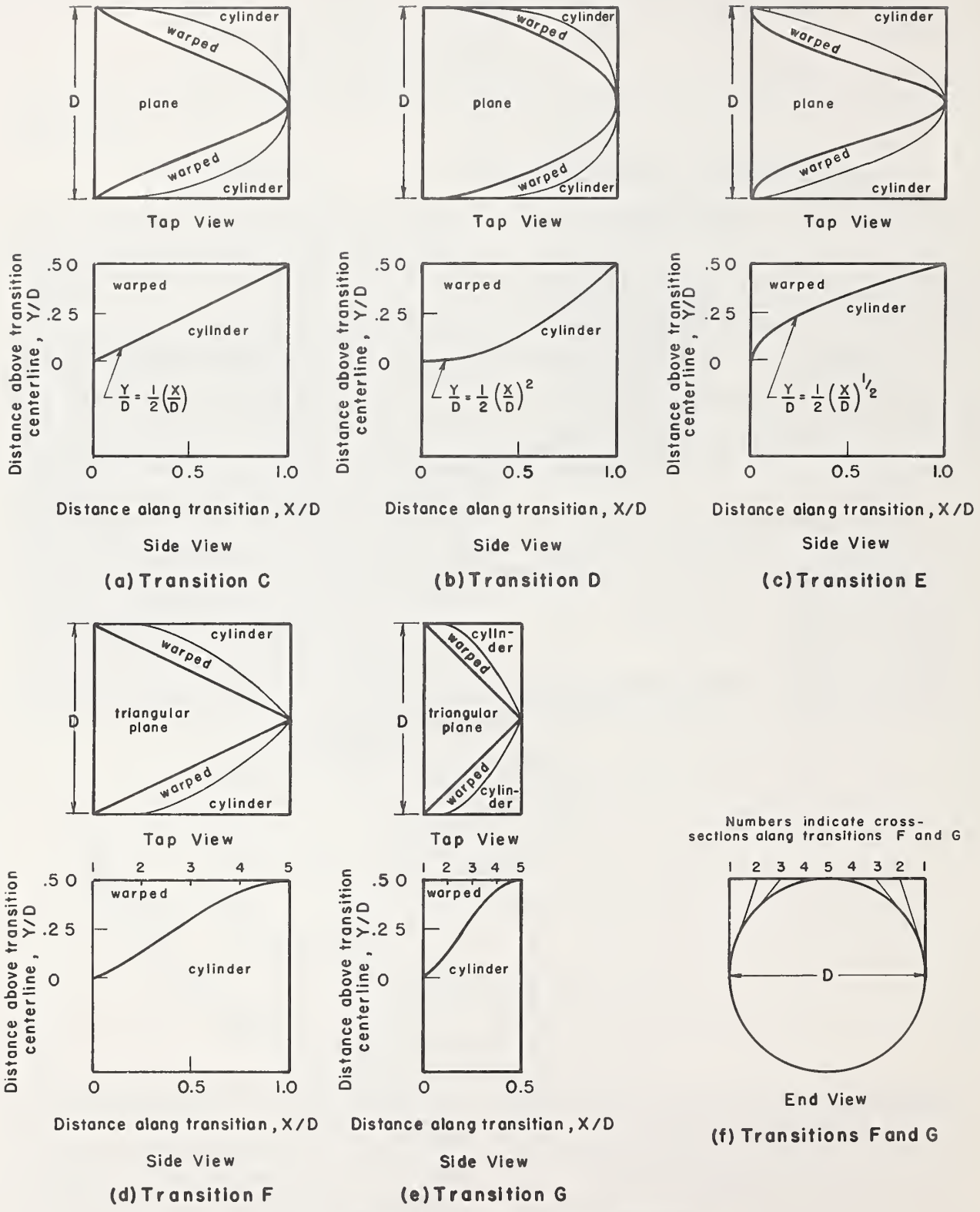

Figure XVI-4.—Warped transition geometries.

surfaces and defined the shape of the plane top.

The formwork required to field-cast these geometries was considered difficult to construct, so an attempt was made to simplify the form of the warped surface.

For the second method, the transition section was defined by specifying the shape of the plane top. Transitions F and G are similar as shown in figures XVI-4(d) and (e). Transition F is 1**D** long and transition G is **D**/2 long—the shortest transition tested. The top of the transition was made an isosceles triangle with a **D**-wide base at the elbow exit and its apex at the downstream end of the transition. Successive lines from the sides of the triangular top, normal to the barrel axis and tangent to the barrel circumference, formed the warped surfaces. The length of each tangent is equal to the half-width of the triangular top at the point from which it is dropped, so the geometry of this warped transition is easier to define and construct than that of the original warped section.

For the conical transition, there is an abrupt adverse angle between the downstream end of the cone and the barrel that may cause flow separation and a low pressure region where cavitation may occur. For the warped transition, all changes in the wall alignment are gradual curves and the tendency for flow separation from the wall is thereby reduced. For these reasons, the form of the warped transition is hydraulically superior to that of the conical transition.

EXPERIMENTAL PROGRAM

Evaluation of the elbow and transition geometries was conducted using both water and air as the test fluids. To expedite the evaluation of the elbows and transitions, all the proposed forms were first tested using air. (For an explanation of testing with air and its advantages see Part XI. A disadvantage of testing with air is that only full conduit flow conditions can be evaluated.) From an analysis of the air test results, the superior elbow and transition designs were selected for further tests using water. Selected for further tests were elbows 3 and 6 and transitions A and F.

Testing with water permitted the evaluation of the hydraulic performance of the two-way drop inlet with the selected elbows and transitions over the entire range of flows. (For an explanation of tests with water see Part X.)

The above tests were made using a circular barrel and semicylindrical drop inlet, elbow, and transition inverts. A second phase of the water tests was conducted using a square barrel. For this phase of the test program the invert cross section of the drop inlets and elbows were semisquare. This resulted in a square cross section at the elbow exit, so a transition between the elbow and the barrel was not necessary. Corresponding air tests were not made.

Elbow and Transition Combinations Tested

The elbow and transition combinations tested are listed in table XVI-3. To evaluate the various elbows, each elbow was tested with transition A. Similarly, to evaluate the transitions, each transition was tested with elbow 3. In addition, transition F was evaluated with elbows 4 and 6. Since each elbow-transition combination was tested with four lengths of drop inlet, the air tests comprised 56 combinations of drop inlet length, elbow shape, and transition form.

Twenty-four series of tests were made using water. For the circular barrel, both elbows 3 and 6 were tested with transitions A and F and the four drop inlet lengths. For the square barrel, the four drop inlet lengths were tested with elbows 3 and 6.

In all, 80 combinations and 88 series are summarized in table XVI-3, triplicate tests having been made of the elbow 3-transition F combination.

TABLE XVI-3.—*Elbow-transition combinations tested*[1]

Fluid	Air							Water	
Barrel	Circular								Square
Elbow	Transition								
1	A	—	—	—	—	—	—	—	—
2	A	—	—	—	—	—	—	—	—
3	A	B	C	D	E	F	G	A	F	None
4	A	—	—	—	—	F	—	—	—	—
5	A	—	—	—	—	—	—	—	—	—
6	A	—	—	—	—	F	—	A	F	None

[1] Each combination was tested with drop inlets 1.5**D**, 2**D**, 3**D**, and 5**D** long.

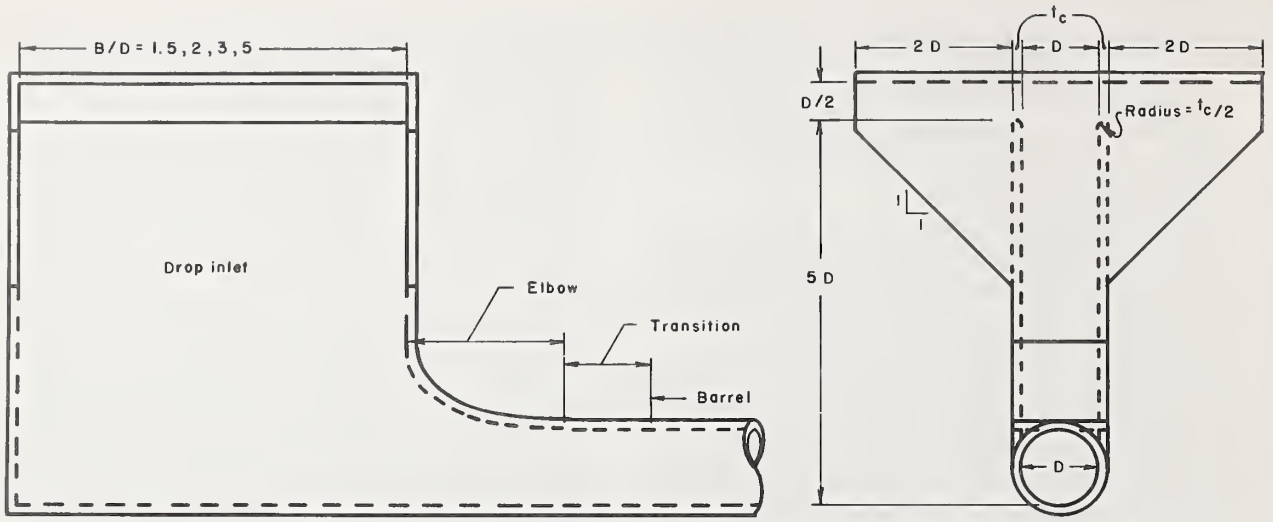

Figure XVI-5.—Two-way drop inlet with semicylindrical invert and elbow-transition barrel entrance.

Discharge

For the air tests, seven different discharges were used, the maximum being limited by the test apparatus. For the water tests, the discharge was varied from a low weir flow to the maximum permitted by the test apparatus.

Drop Inlets

The drop inlets used for the tests are shown in figure XVI-5. The cross section dimensions were identical for each of the four drop inlets built with different lengths. The dimensions used were taken from drawing ES-150 "Drop Inlet Spillways. Standard for Covered Top Risers."[11] However, no trashrack was used.

Conduit Slope

As shown in table XVI-1, except for elbow 4 the conduit slope was zero—the same as that of the inverts of the drop inlet, elbow, and transition. Table XVI-1 shows that the slope used with elbow 4 is 0.025. This slope began at the drop inlet exit and continued through the elbow, transition, and barrel.

The Models

A typical air model is shown in figure XVI-6. The dimensions are given in figure XVI-5 and tables XVI-1 and XVI-2. A longer-than-needed drop inlet was available from earlier tests. The drop inlet lengths for the current tests were obtained by installing intermediate upstream endwalls. As can be seen in figure XVI-6, the downstream endwall and the elbows were installed at the downstream end of the over-long drop inlet. A removable, semicylindrical invert was used for the drop inlet and elbow. Each transition was attached to the elbow exit. A 2**D**-length of barrel was made a part of each transition. Figure XVI-6 also shows the numerous piezometers used to monitor the pressures throughout the spillway entrance.

A typical water model is shown in figure XVI-7. The dimensions are given in figure XVI-5 and tables XVI-1 and XVI-2. A similar drop inlet was built for each drop inlet length. Two drop inlet inverts were provided for each drop inlet length. Shown is a semicylindrical invert. The other invert was a semisquare box.

Each elbow section was constructed in two parts as shown typically in figure XVI-8. Semicylindrical and semisquare box inverts were made for each elbow so the same elbow could be tested for both circular and square barrels. Each elbow crown section was fitted to the semicylindrical and semisquare box inverts and each assembly fitted to each length of drop inlet.

Transitions were required only for circular barrels, so each transition was made as a complete unit and fitted to each elbow tested. A 2**D** length of barrel was made a part of each transition. Typical transitions are shown in figure XVI-9.

[11] Young, G. Preparation of National Standard Detail Drawings for Pipe Drop Inlet Principal Spillways, U.S. Department of Agriculture, Soil Conservation Service, Washington, D.C., Engineering Memorandum SCS-50, May 16, 1963, 2 pp., 7 illus.

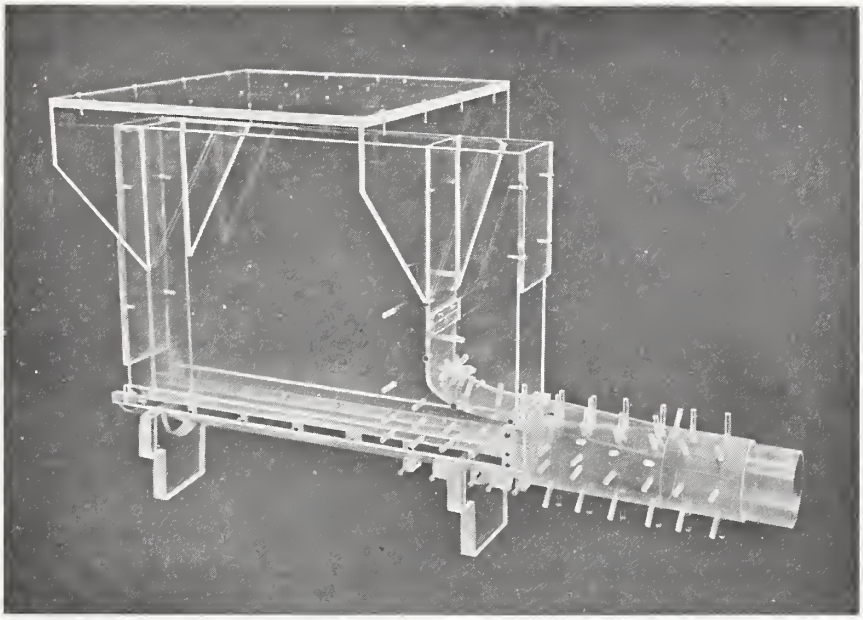

Figure XVI-6.—Typical two-way drop inlet with elbow 1 and transition A used for air tests.

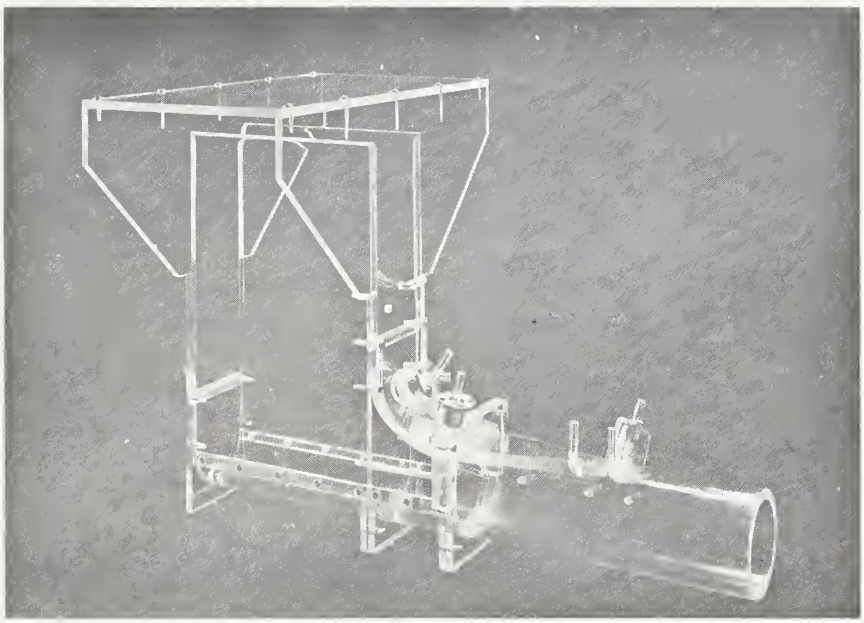

Figure XVI-7.—Two-way drop inlet 3D long with double circle elbow 6 and conical transition A used for water tests.

The transparent thermoplastic for the elbows and transitions was heated and shaped on carefully machined renwood (artificial wood) forms. After cooling, the elbows and transitions were kept on the forms during machining so they would retain their shape until assembled.

TEST APPARATUS AND TEST PROCEDURE

Air Tests

The air apparatus and test procedure have been described in Part XI. The barrel diameter D was 3 in (7.62 cm).

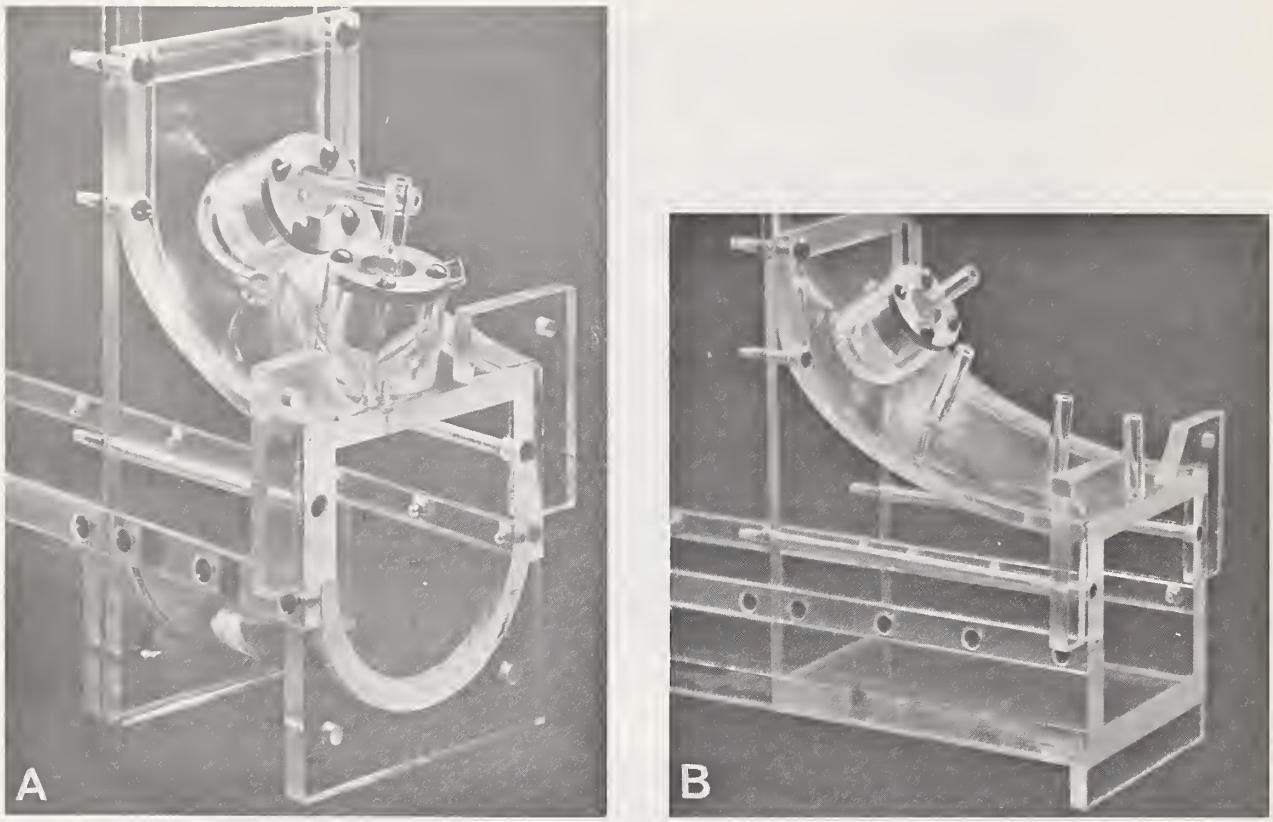

Figure XVI-8.—The elbow section. (A) Double circle elbow 6 with semicylindrical invert. (B) Elliptical elbow 3 with semi-square box invert.

Water Tests

Elbows 3 and 6 and transitions A and F were tested with water using the apparatus and procedures described in Part X. Both 2.25 in (5.72 cm) circular and 2.25 in (5.72 cm) square conduits were used. The drop inlets, elbows, and transitions were geometrically similar to their corresponding air models. Pressures were measured at fewer—but similar—locations.

Because the conduits had zero slope, the head available was insufficient to obtain Reynolds numbers comparable to those of the air tests. To verify the effect of Reynolds number on the pressure characteristics of the elbows and transitions, the same range of Reynolds numbers had to be used in the water model as had been used in the air model. To increase the Reynolds numbers, the available head was increased by means of a controlled flow return line between the conduit exit and the water storage reservoir. Adjustment of a control valve in the return line simulated sloping the barrel to change the effective head on the spillway.

The piezometers at the locations of minimum average pressures on each elbow and transition were equipped with a mounting for a strain-gage type piezoelectric cell. These mountings are evident in figures XVI-7, XVI-8, and XVI-9. Pressure cells with a range of ± 2.5 lb/in^2 (± 17.2 kn/m^2) were used to monitor the instantaneous pressure fluctuations at these locations.

After installing each cell, the pressure chamber was carefully cleared of air, the output signal was calibrated with a known pressure change, and the recording system was zeroed and referenced to a known water surface elevation. A direct-writing oscillograph recorded the fluctuation data on temperature-sensitive paper.

ANALYTICAL METHODS

Although some variations and additions were made, the analytical methods used were the same as those described in Parts XI and X for the air and water tests, respectively.

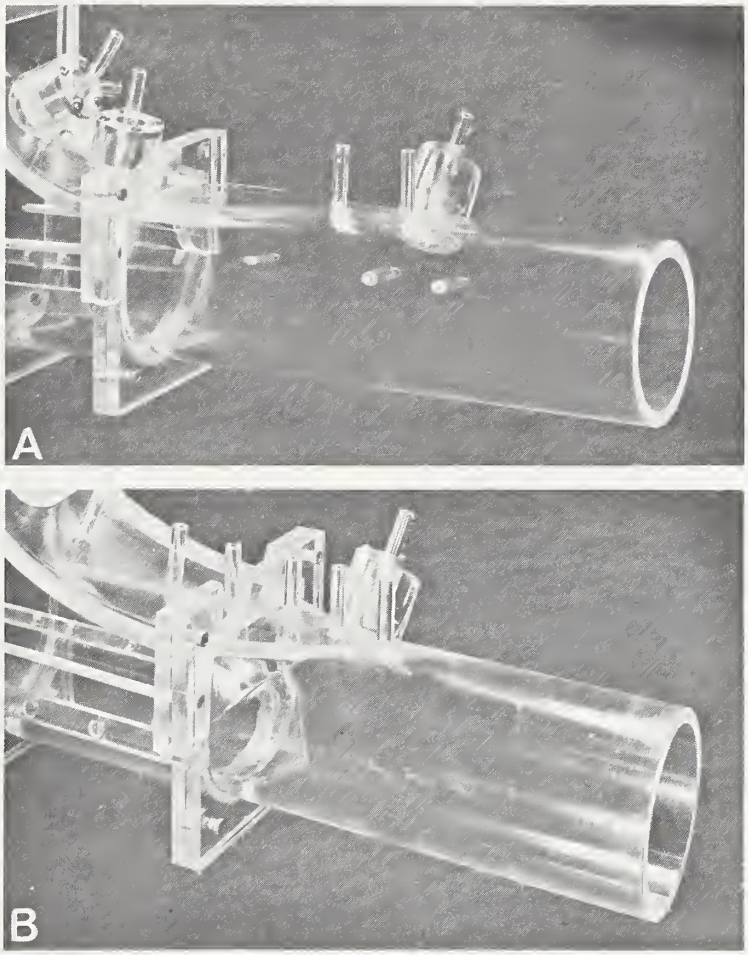

Figure XVI-9.—Transitions from semicylindrical inverts and semisquare crowns at elbow exit to circular barrel. (A) Conical transition A with double circle elbow 6. (B) Warped transition F with elliptical elbow 3.

The pressure fluctuation data was analyzed manually. The average pressure at each pressure cell location was determined from the record trace for each run and compared with the average piezometric pressures at the same locations. The charts were scanned to determine the average maximum fluctuations from the average pressures, particularly the negative fluctuations which most directly indicate the cavitation potential.

TEST RESULTS

The six elbow and seven transition designs were tested to find the form and proportions of practical and hydraulically efficient elbows and transitions between the two-way drop inlet and the circular closed conduit spillway barrel. These designs were first tested with air to determine the pressure coefficients, the pressure gradients along each of the sections, and the energy loss coefficients for various entrance geometries. In this preliminary investigation, elbows 3 and 6 and transitions A and F performed satisfactorily.

Subsequent tests were made with elbows 3 and 6 and transitions A and F using water. The subsequent tests were made to check the hydraulic performance of the two-way drop inlet with these elbows and transitions, and to measure pressures and pressure fluctuations at points of minimum average pressure.

Elbows 3 and 6 were also evaluated as the junction between the two-way drop inlet with a flat bottom and a square barrel closed conduit spillway.

The pressures and the energy losses will be considered in separate sections.

Pressures

Each elbow and transition was evaluated on the basis of the pressures and the pressure gradient along the elbow, the transition, and in the barrel near its entrance. This report section will present the results of the investigations of the average and instantaneous pressures throughout the barrel entrance region for each geometry tested.

Instantaneous pressures are important because turbulence causes fluctuations of the pressure above and below the average pressure. The negative pressure fluctuations increase the cavitation potential by momentarily lowering the pressure. If the pressure at a point is reduced to the vapor pressure, cavitation can be initiated even though the average pressure at the point is above the cavitation level. Prolonged intermittent occurrences of cavitation may eventually cause structural damage if the phenomena is concentrated at a location. Therefore, during the water tests, information was obtained to evaluate the cavitation potential by monitoring the pressure fluctuations at the locations of minimum average pressure coefficients for elbows 3 and 6 and transitions A and F.

The pressures were analyzed in terms of a pressure coefficient. The pressure coefficient for any point **n** is defined as h_n/h_{vp} where h_n is the difference between the hydraulic gradeline and the projected barrel friction gradeline at **n** and h_{vp} is the velocity head in the barrel. The barrel friction gradeline was determined by using the least squares method.

The combinations of drop inlet lengths, elbows, and transitions tested are given in table XVI-3.

Effect of discharge

For each elbow-transition combination, seven different air discharges were used to obtain a range of the Reynolds number. For each discharge the pressures in the elbow, transition, and barrel entrance region and the barrel itself were expressed as pressure coefficients, h_n/h_{vp}. The computer output from series B-113 shown in table XVI-4 is typical. Each column gives the results for one discharge—and Reynolds number $R = V_pD/\nu$. The pressure coefficients for each piezometer location for each run are listed across the table for easy comparison.

Looking across the table along the lines numbered 1 to 72 in the left column, the pressure coefficients for each of the 72 piezometer locations are seen to be the same within the experimental precision achieved. The average of the coefficients at each location is given in the right column. This observation means that the deviation of the hydraulic gradeline from the projected barrel friction gradeline is directly proportional to the barrel velocity head, so the ratio h_n/h_{vp} is a constant for each location in the spillway for any given geometry. The water tests gave the same results. As a result all pressure coefficients used in the subsequent analyses are the average for each spillway geometry of all the coefficients obtained at each piezometer location.

Pressure coefficients

The average pressure coefficients from all the tests will be presented before discussing the effects of the spillway geometry on the pressures. The pressure coefficients obtained during both air and water tests are shown for the 3**D**-long drop inlet, elbow 3, and transition A in figure XVI-10. The coefficients are given in their respective vertical and longitudinal locations on this side view of the spillway entrance region, but the pressures were measured on the periphery as illustrated in figure XVI-6. The two locations along the crown of the transition with two values indicate that there were two piezometers on the plane top at the same section.

Eighty figures would be required to present the results as in figure XVI-10 for all the combinations listed in table XVI-3. Therefore, only the coefficients along the centerline of the crown and the invert—plus any other coefficients indicative of low pressures—will be given. The test results for each elbow-transition combination and all four drop inlet lengths will be given on individual plots.

The pressure coefficients for elbows 1 through 6 tested with transition A are used to compare the characteristics of the elbows. The results are shown in figure XVI-11. The data for transitions B through G with elbow 3 shown in figure XVI-12 plus that for transition A with elbow 3 in figure XVI-11(c) are used to compare and evaluate the transitions. The results for two other combinations, elbows 4 and 6 with transi-

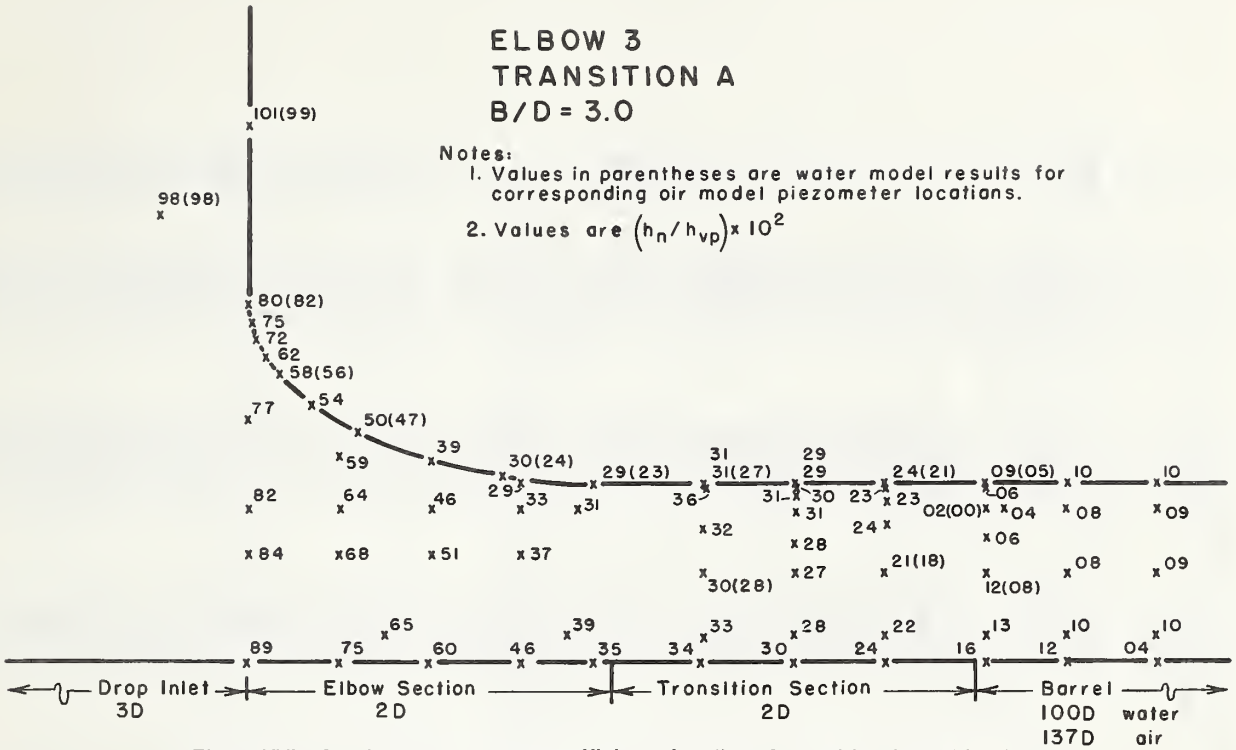

Figure XVI-10.—Average pressure coefficients for elbow 3-transition A combination.

tion F, are shown in figure XVI-13. The pressure coefficients for elbows 3 and 6 with the square conduit are presented in figure XVI-14.

The piezometer locations are measured from the upstream end of the elbow section in dimensionless form as **x/D** where **x** is the horizontal distance from the elbow entrance to the piezometer. In the discussion of the transition pressures, the location of the pressure coefficients will be referenced to the upstream end of the transition.

A common symbol definition was adopted for figures XVI-11 through XVI-14. The pressure coefficients along the crown and the invert for the air tests are represented by open and closed symbols, respectively. The half-closed symbols represent pressure coefficients along the crown for the water tests. Slashed symbols represent minimum average pressure coefficients at specified locations.

The solid symbols show that the invert pressure coefficients along the elbows and transitions are always above the friction gradeline and equal to or greater than the crown coefficients. Because the lower crown pressures present the greater potential for pressure problems, the crown pressures were used for all analyses.

Effect of drop inlet length

The plots of h_n/h_{vp} along each of the elbows presented in figure XVI-11 illustrate the variation of the pressure coefficient at each piezometer location as the drop inlet length increases from 1.5**D** to 5**D**. The variation in h_n/h_{vp} caused by the change in drop inlet length is large near the upstream end of the elbows but diminishes with distance into the entrance for all geometries.

For **x/D** $\lesssim$ 1/3 the elbow crown pressure coefficients increase with the drop inlet length. At **x/D** $\simeq$ 1/3 the pressure coefficients for each elbow approach a common value for all four drop inlet lengths.

For **x/D** > 1/3, the effect of drop inlet length reverses and the coefficients at each of the piezometer locations decrease as the drop inlet length increases from 1.5**D** to 5**D**.

The average crown pressure coefficients along each of the transitions A through G-elbow 3 combinations are plotted in figures XVI-11(c) and XVI-12. These plots show that the pressure coefficients throughout all the transitions are consistently higher with the shorter drop inlets than with the longer ones by 0.1 velocity heads or less.

Table XVI-4.—*Typical computer printout for air tests*

AGRICULTURAL RESEARCH SERVICE
AIR MODEL TEST RESULTS

SERIES B- 113

RUN NO,	1	2	3	4	5	6	7	Average
P2/P1	0,922	0,933	0,945	0,965	0,915	0,925	0,947	
W	0,586	0,546	0,500	0,406	0,391	0,370	0,315	
F	0,015	0,015	0,016	0,016	0,016	0,017	0,017	
R	245766,514	229109,589	209240,521	170461,624	163367,427	154322,806	131834,144	
D/2 TOP	-4,233	-5,033	-6,207	-9,907	-10,728	-12,112	-17,301	
D/2 BOT	-4,233	-5,033	-6,207	-9,907	-10,728	-12,112	-17,301	
17D	0,007	0,009	0,005	0,020	0,015	0,015	0,009	
33D	-0,003	-0,006	-0,004	-0,002	0,003	-0,001	-0,006	
49D	0,004	0,003	0,003	-0,003	-0,000	0,004	0,010	
65D	-0,004	-0,001	-0,000	-0,001	-0,001	-0,003	-0,008	
81D	0,004	0,006	0,003	0,008	-0,007	0,006	-0,000	
97D	0,002	0,004	0,002	0,000	0,006	-0,004	0,005	
113D	-0,005	-0,005	-0,004	0,002	-0,001	-0,007	0,004	
129D	0,007	0,004	0,004	0,003	-0,000	0,005	-0,002	
137D	-0,005	-0,005	-0,004	-0,007	0,001	0,001	-0,002	
KE	0,243	0,245	0,262	0,294	0,269	0,274	0,277	0,27
KC	2,220	2,287	2,321	2,193	2,158	2,233	2,310	2,25
KT	0,095	0,092	0,107	0,147	0,123	0,123	0,121	0,12
PA	2059,844	2057,026	2054,727	2038,190	2035,188	2035,892	2033,074	
A	2019,139	2021,678	2024,837	2018,039	2016,790	2019,384	2021,238	
B	-2,091	-1,850	-1,561	-1,053	-0,984	-0,887	-0,658	
W 137D	0,068	0,068	0,068	0,069	0,069	0,069	0,069	
HV 137D	32,980	28,560	23,812	15,631	14,552	13,001	9,294	
1	0,963	0,960	0,973	1,011	0,987	0,980	0,982	0,98
2	0,752	0,753	0,767	0,788	0,765	0,771	0,775	0,77
3	0,803	0,801	0,811	0,844	0,817	0,819	0,822	0,82
4	0,826	0,823	0,837	0,868	0,838	0,843	0,848	0,84
5	0,875	0,874	0,890	0,916	0,893	0,899	0,897	0,89
6	0,583	0,570	0,592	0,618	0,594	0,579	0,583	0,59
7	0,628	0,624	0,639	0,666	0,646	0,641	0,643	0,64
8	0,670	0,665	0,679	0,705	0,684	0,689	0,683	0,68
9	0,732	0,730	0,745	0,773	0,748	0,751	0,755	0,75
10	0,642	0,634	0,650	0,674	0,654	0,655	0,652	0,65
11	0,452	0,445	0,452	0,475	0,458	0,454	0,458	0,46
12	0,501	0,491	0,512	0,535	0,513	0,511	0,498	0,51
13	0,586	0,584	0,598	0,623	0,603	0,606	0,607	0,60
14	0,320	0,310	0,327	0,352	0,334	0,329	0,327	0,33
15	0,364	0,360	0,374	0,396	0,372	0,376	0,369	0,37
16	0,449	0,446	0,464	0,484	0,470	0,476	0,465	0,46
17	0,382	0,377	0,397	0,409	0,394	0,401	0,392	0,39
18	0,300	0,283	0,339	0,323	0,306	0,316	0,300	0,31
19	0,340	0,333	0,352	0,371	0,360	0,360	0,354	0,35

h_t/h_{vp} for barrel

h_x/h_{vp} for drop inlet, elbow, transition, and barrel entrance

20	0.983	0.986	1.005	1.036	1.013	1.012	1.022	1.01
21	0.280	0.274	0.284	0.303	0.296	0.303	0.293	0.29
22	0.783	0.779	0.798	0.824	0.804	0.805	0.808	0.80
23	0.742	0.738	0.760	0.773	0.757	0.758	0.755	0.75
24	0.699	0.698	0.714	0.734	0.720	0.725	0.723	0.72
25	0.612	0.606	0.621	0.644	0.627	0.631	0.624	0.62
26	0.566	0.561	0.582	0.599	0.579	0.586	0.587	0.58
27	0.525	0.519	0.537	0.556	0.541	0.543	0.545	0.54
28	0.486	0.482	0.502	0.519	0.500	0.502	0.505	0.50
29	0.379	0.371	0.385	0.402	0.388	0.394	0.392	0.39
30	0.289	0.286	0.297	0.311	0.294	0.307	0.307	0.30
31	0.282	0.278	0.284	0.302	0.287	0.298	0.298	0.29
32	0.300	0.298	0.312	0.333	0.317	0.317	0.318	0.31
33	0.302	0.300	0.304	0.333	0.317	0.317	0.318	0.31
34	0.340	0.337	0.351	0.369	0.364	0.370	0.364	0.36
35	0.300	0.300	0.312	0.333	0.317	0.327	0.324	0.32
36	0.297	0.291	0.299	0.322	0.308	0.312	0.304	0.30
37	0.314	0.315	0.323	0.341	0.329	0.336	0.331	0.33
38	0.331	0.327	0.339	0.362	0.346	0.354	0.347	0.34
39	0.276	0.279	0.286	0.306	0.295	0.297	0.300	0.29
40	0.284	0.282	0.286	0.314	0.295	0.297	0.300	0.29
41	0.322	0.288	0.294	0.318	0.304	0.306	0.306	0.30
42	0.297	0.299	0.305	0.326	0.308	0.321	0.313	0.31
43	0.305	0.299	0.310	0.334	0.308	0.321	0.313	0.31
44	0.269	0.264	0.273	0.294	0.278	0.287	0.286	0.28
45	0.261	0.258	0.266	0.294	0.269	0.278	0.273	0.27
46	0.276	0.269	0.279	0.306	0.282	0.282	0.286	0.28
47	0.288	0.283	0.292	0.314	0.295	0.305	0.302	0.30
48	0.228	0.222	0.232	0.255	0.235	0.243	0.242	0.24
49	0.222	0.214	0.229	0.251	0.235	0.234	0.235	0.23
50	0.228	0.218	0.235	0.255	0.235	0.238	0.235	0.23
51	0.235	0.224	0.235	0.267	0.244	0.248	0.248	0.24
52	0.209	0.198	0.214	0.231	0.218	0.210	0.208	0.21
53	0.213	0.198	0.216	0.243	0.218	0.224	0.215	0.22
54	0.231	0.220	0.236	0.256	0.240	0.243	0.238	0.24
55	0.082	0.070	0.087	0.105	0.095	0.085	0.091	0.09
56	0.052	0.042	0.058	0.069	0.065	0.057	0.051	0.06
57	0.031	0.001	0.024	0.037	0.027	0.028	0.017	0.02
58	0.054	0.044	0.064	0.081	0.074	0.066	0.071	0.06
59	0.114	0.101	0.124	0.145	0.133	0.128	0.131	0.12
60	0.114	0.105	0.124	0.145	0.138	0.138	0.138	0.13
61	0.146	0.137	0.157	0.174	0.161	0.168	0.166	0.16
62	0.033	0.021	0.040	0.057	0.043	0.045	0.045	0.04
63	0.085	0.075	0.094	0.109	0.103	0.107	0.106	0.10
64	0.070	0.067	0.081	0.105	0.086	0.093	0.086	0.08
65	0.076	0.067	0.081	0.105	0.086	0.093	0.092	0.08
66	0.087	0.080	0.097	0.121	0.107	0.112	0.112	0.10
67	0.108	0.099	0.118	0.137	0.128	0.135	0.134	0.12
68	0.088	0.081	0.097	0.117	0.103	0.111	0.108	0.10
69	0.084	0.075	0.090	0.105	0.094	0.101	0.094	0.09
70	0.074	0.066	0.090	0.105	0.094	0.097	0.094	0.09
71	0.086	0.077	0.092	0.113	0.098	0.116	0.101	0.10
72	0.034	0.027	0.043	0.062	0.048	0.056	0.046	0.04

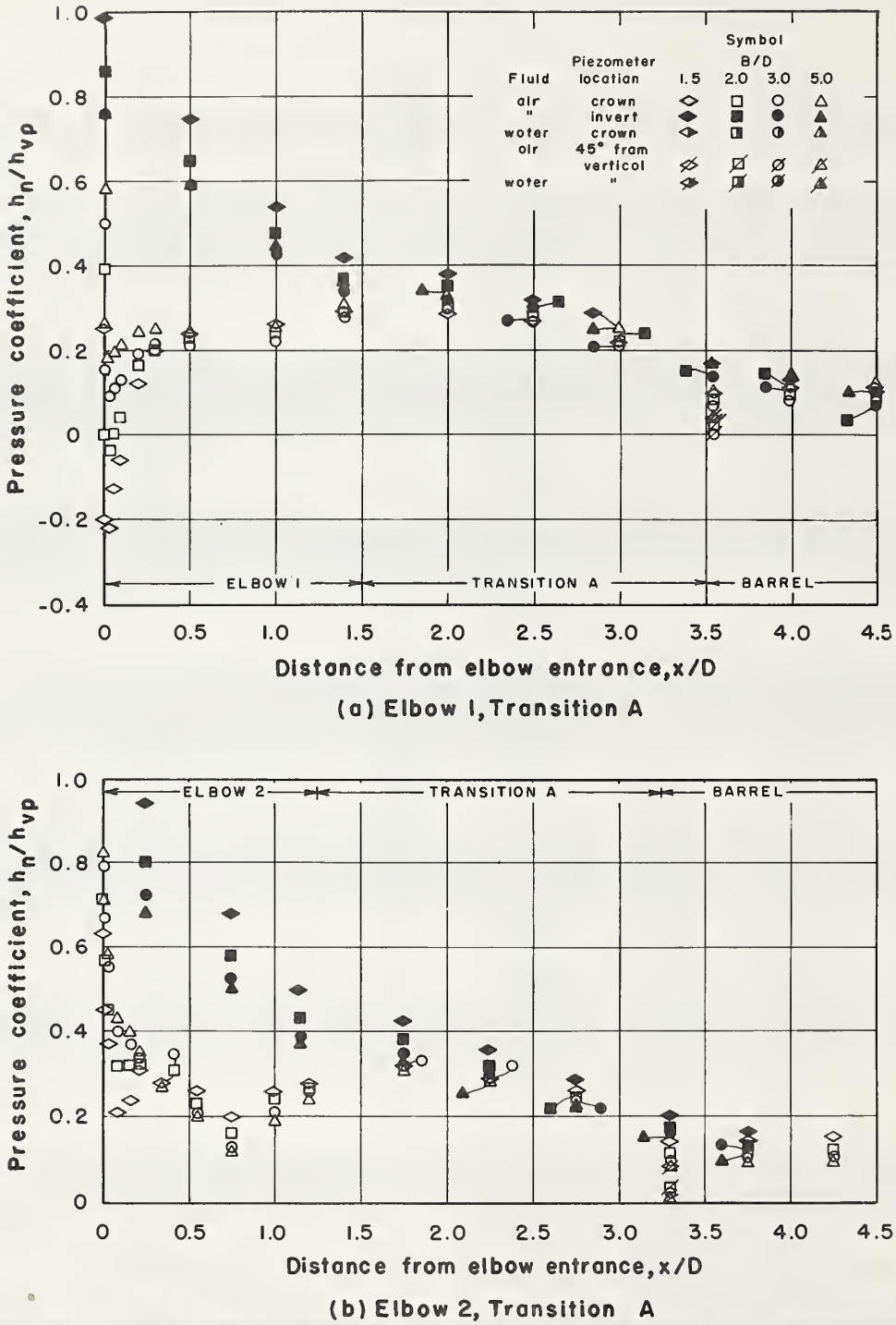

Figure XVI-11.—Pressure coefficients along elbows 1 through 6, transition A, and circular barrel entrance.

The crown pressure coefficients along elbows 3 and 6 with a flat invert and the square barrel are shown in figure XVI-14. The effects of drop inlet length on the pressure coefficients are similar to those for the elbows with semicylindrical inverts.

The variation of the effect of the drop inlet length on the pressure coefficients along the elbow sections may be explained as follows: As the drop inlet length is reduced, the velocity in

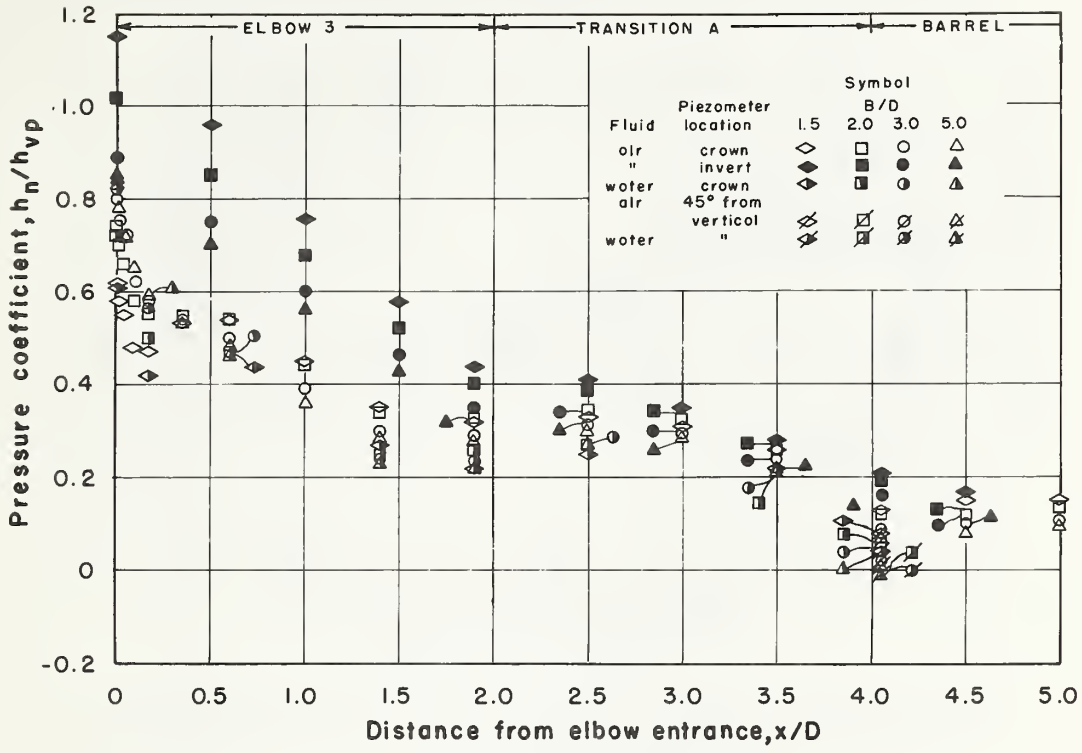

(c) Elbow 3, Transition A

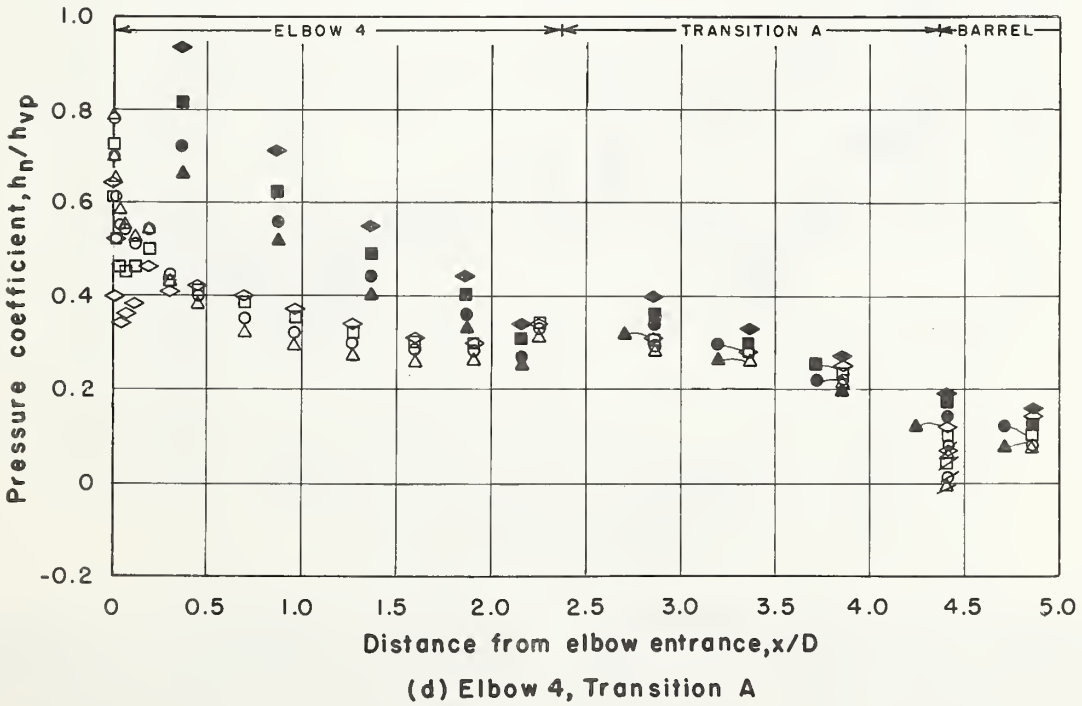

(d) Elbow 4, Transition A

Figure XVI-11.—Continued.

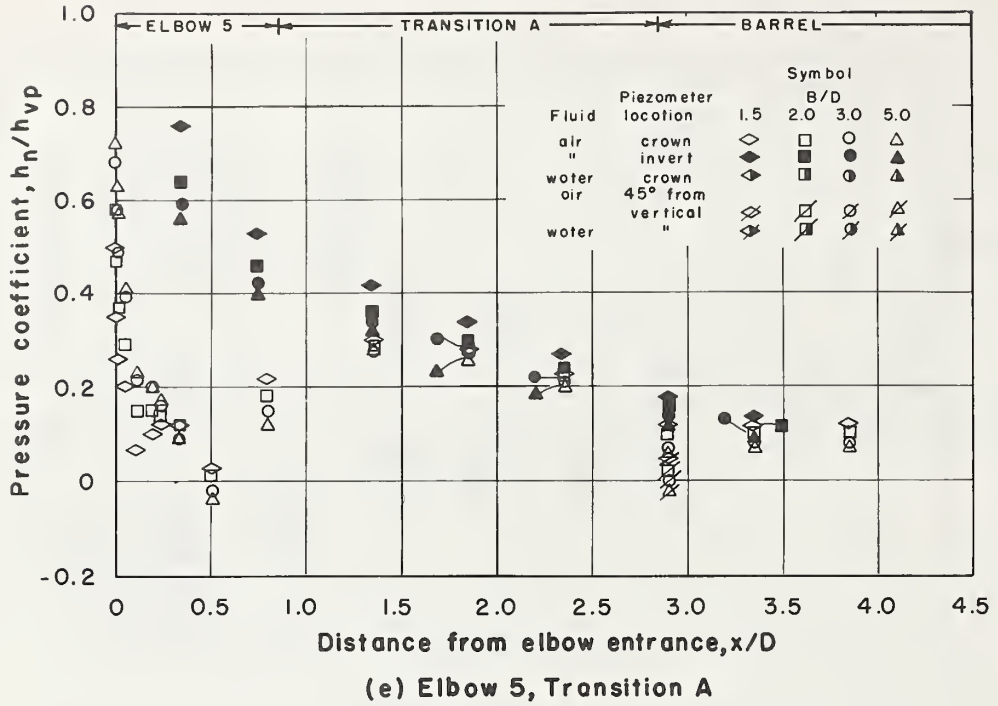

(e) Elbow 5, Transition A

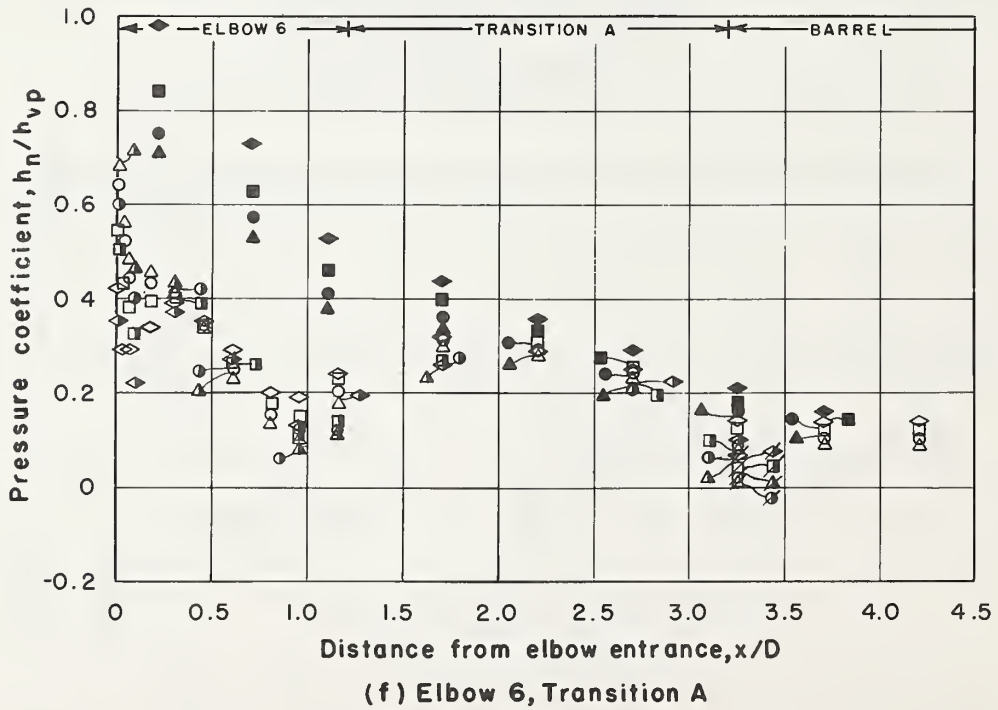

(f) Elbow 6, Transition A

Figure XVI-11.—Continued.

the drop inlet increases for a given discharge and the change in flow direction at the elbow becomes more abrupt. This increases the tendency for flow separation from the upstream part of the elbow, causes the decrease in h_n/h_{vp} at the elbow entrance as the drop inlet shortens, and directs the flow jet toward the invert. The flow jet is then reflected from the invert back toward the crown. The shorter the drop inlet the stronger the reflection, which ex-

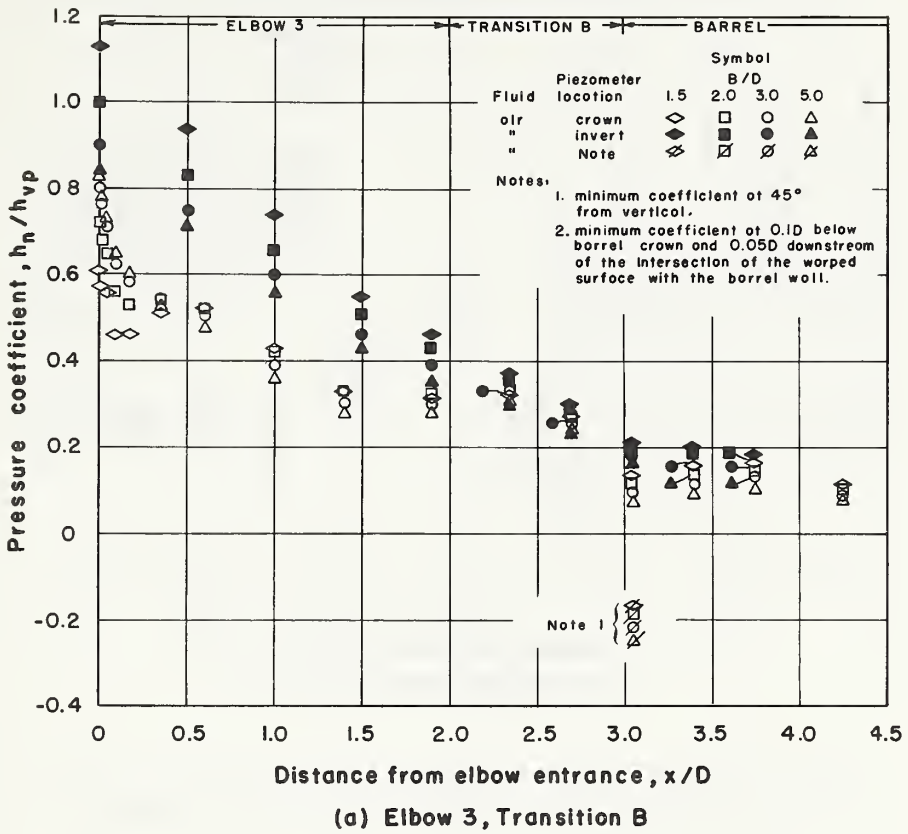

(a) Elbow 3, Transition B

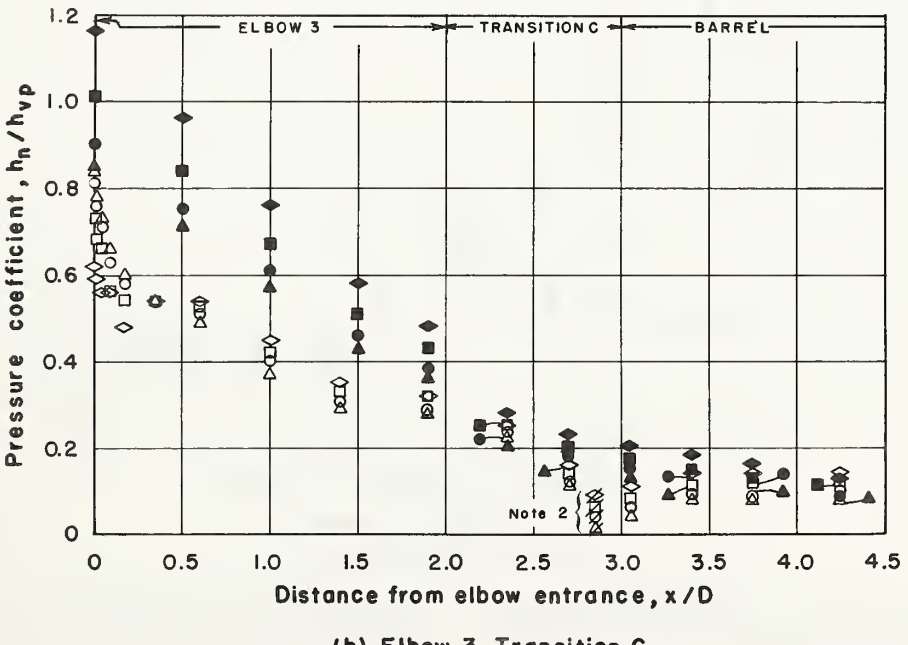

(b) Elbow 3, Transition C

Figure XVI-12.—Pressure coefficients along transitions B through G, elbow 3, and circular barrel entrance.

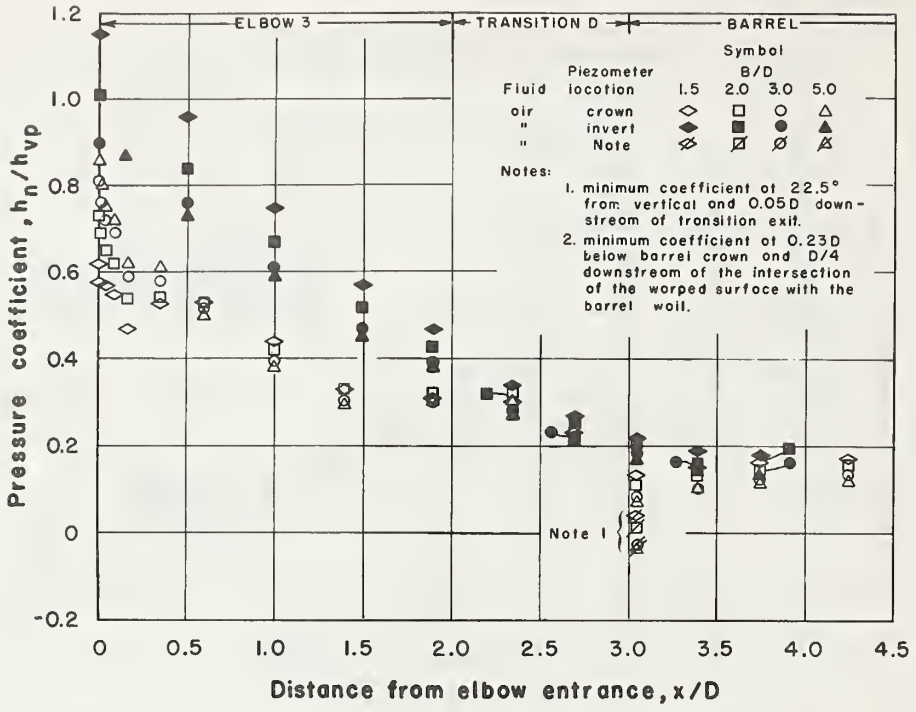

(c) Elbow 3, Transition D

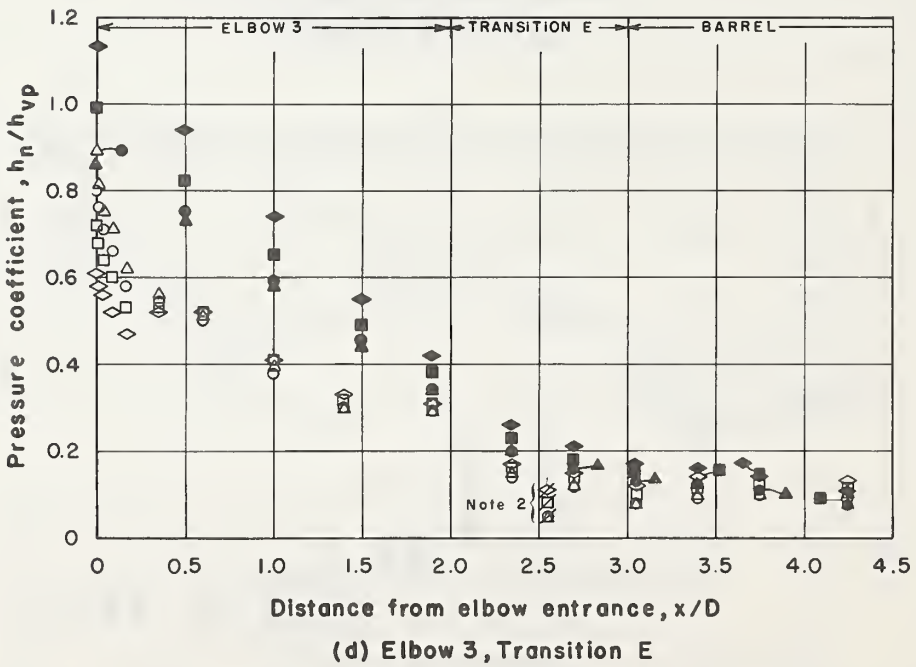

(d) Elbow 3, Transition E

Figure XVI-12.—Continued.

plains the reversal of the effect of the drop inlet length on h_n/h_{vp} downstream of $x/D \simeq 1/3$.

Performance criteria

The pressure coefficients are used to evaluate and to compare the performances of the elbows and transitions. To reduce the likelihood of cavitation, a high minimum pressure coefficient is desirable.

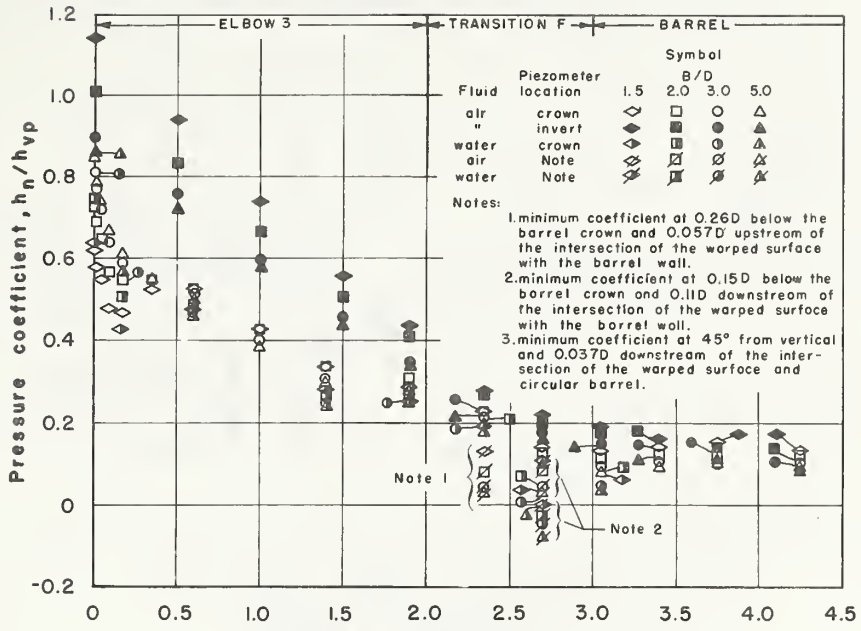

(e) Elbow 3, Transition F

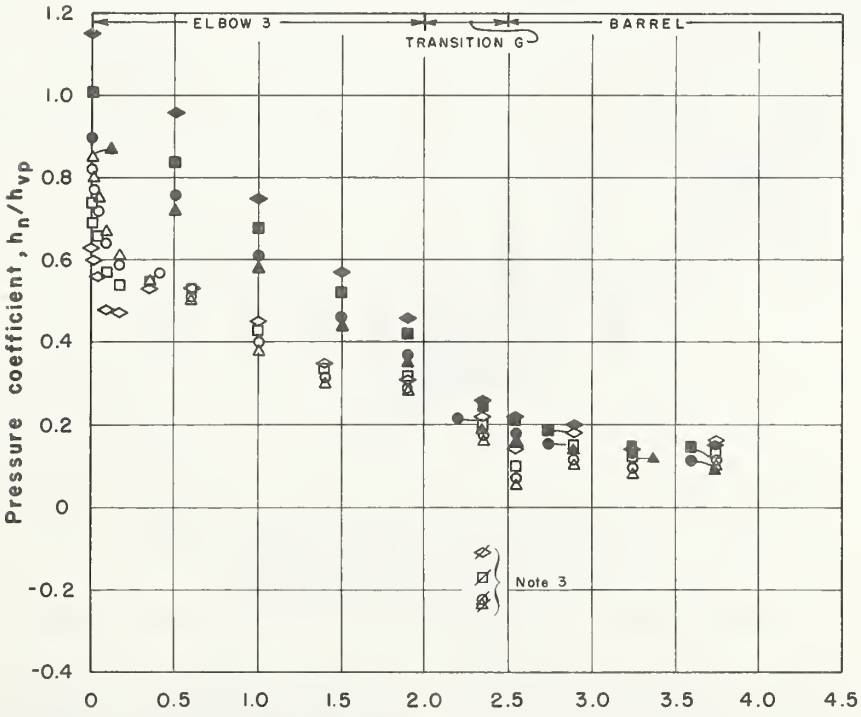

(f) Elbow 3, Transition G

Figure XVI-12.—Continued.

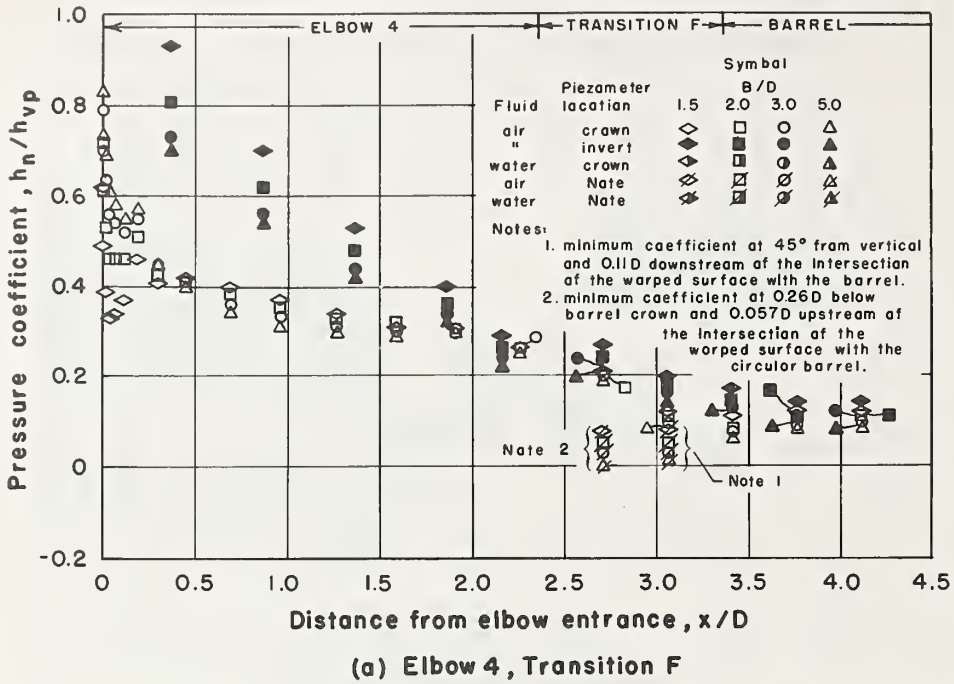

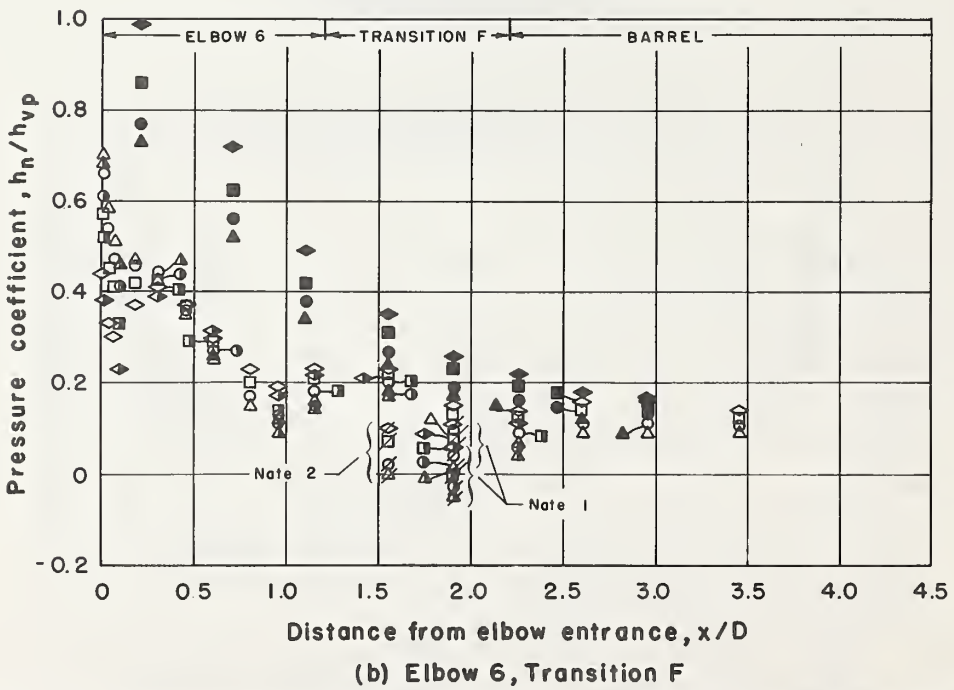

Figure XVI-13.—Pressure coefficients along elbows 4 and 6, transition F, and circular barrel entrance.

Because the flow area decreases along the elbows and transitions, there is an accompanying increase in velocity and a decrease in pressure. A smooth curve of steadily decreasing pressures—a "favorable" pressure gradient—indicates a good form.

When the pressure increases with distance along the elbows and transitions, the pressure gradient is "adverse." Although some adversity in the pressure gradient can be tolerated, an adverse pressure gradient is usually undesirable. The vapor bubbles formed in a region

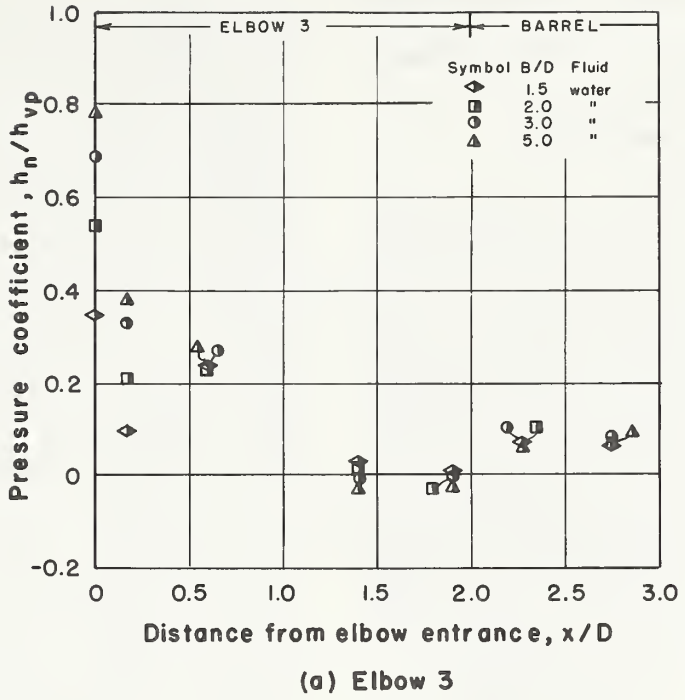

(a) Elbow 3

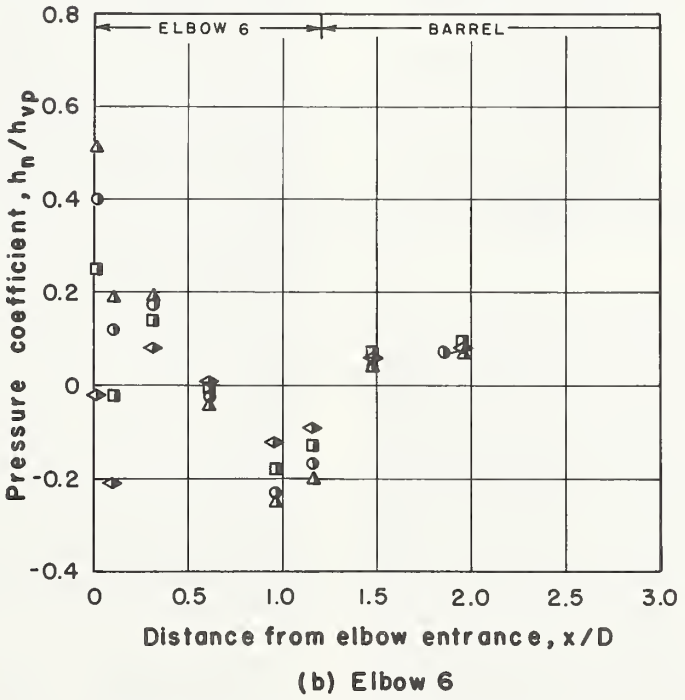

(b) Elbow 6

Figure XVI-14.—Pressure coefficients along crown of elbows 3 and 6 and square barrel entrance.

where the pressure is the vapor pressure will collapse when the pressure increases sufficiently in a following adverse pressure gradient. The conduit may be damaged if the bubbles collapse on the conduit wall rather than within the fluid. Furthermore, an adverse pressure gradient is an indication of possible separation of the flow from the conduit boundary with atten-

dant turbulent eddies and an increase in energy losses.

The elbows and transitions will be evaluated using the above criteria.

Elbow Evaluation

Free streamline elbow 4

This elbow will be discussed first because the free streamline elbow presumably represents the best shape. As such, the pressures and pressure gradients should approximate the ideal. The measured differences will be used to show how far the pressures and pressure gradients for this elbow differ from the "ideal," and will provide a base for comparisons with other elbows. Differences between the assumption of an ideal fluid by Michell[12] in his derivation of the free streamline shape and the real fluid used in the model produced other than ideal pressures along elbow 4. These differences are:

Michell's Assumptions	*Model Difference*
Two-dimensional flow	Base of drop inlet is semicylindrical
Frictionless boundaries	Friction on boundaries, side boundaries only 1**D** apart
Incompressible fluid	No significant difference
Non-turbulent flow	Strong turbulence in drop inlet
Profile computed for **B/D** = 2	Profile incorrect for **B/D** = 1.5, 3, and 5
Pressure and velocity are constant along the free streamline (elbow curvature)	Measured pressures are not constant

Because the free streamline is **D**/2 or more above the pipe centerline and the geometry above the centerline is two-dimensional, the difference from two-dimensional flow is probably small. Because there is boundary friction in the model, the model differs from the assumption. In addition, the relatively close spacing of the side boundaries magnifies the effect of boundary friction. An important difference may be the highly turbulent flow in the model drop inlet. And of course a profile designed for **B/D** = 2 cannot be expected to give correct boundary pressures for other drop inlet lengths. Therefore, the pressures along the free streamline elbow can be expected to differ from the constant pressure expected if all of Michell's assumptions had been met.

[12] See footnote 8.

The degree to which the differences between the model and the assumptions affected the pressures along elbow 4 is shown in figures XVI-11(d) and XVI-13(a). There is an adverse (increasing) pressure gradient that reaches a maximum at **x/D** = 0.19—close to the elbow entrance. This adverse pressure gradient, which exists even for the long 3**D**- and 5**D**-long drop inlets, is pronounced for the 2**D**-long drop inlet for which the elbow is built and is greatest for the short 1.5**D**-long drop inlet. However, all pressures are positive with respect to the extended barrel friction gradeline, so pressures that might cause cavitation damage do not exist. Nevertheless, the tests show that differences between Michell's assumptions and the model affect the pressures and indicate that designing an elbow for a drop inlet length less than actually exists will reduce the extent of the adverse pressure region.

The rapid drop in pressures near the elbow entrance and subsequent increases in the pressure indicates that the rate of curvature near the entrance is too great and that at least a tendency exists for separation of the flow from the boundary. The great effect of drop inlet length on the free streamline shape is shown in figure XVI-15. These curves support the above statement and the test results show that designing a free streamline elbow for a shorter drop inlet length than actually exists will decrease the adverse pressure region and overcome some of the differences between Michell's assumptions and the elbow modeled.

The pressure gradient for the free streamline elbow became favorable again and much milder beyond **x/D** = 0.19 for all drop inlet lengths and remained so for the elbow 4-transition F combination as shown in figure XVI-13(a). However, as shown in figure XVI-11(d) for the elbow 4-transition A combination, the pressure gradient became adverse again beyond **x/D** = 1.92. This difference may be caused by the higher entrance pressure for transition A than for transition F.

Although the pressure characteristics of free streamline elbow 4 are less than ideal, the results indicate that this profile is satisfactory if its long length is acceptable.

Elliptical elbows 1, 2, and 3

Three elliptical profiles were tested before obtaining satisfactory pressure characteristics.

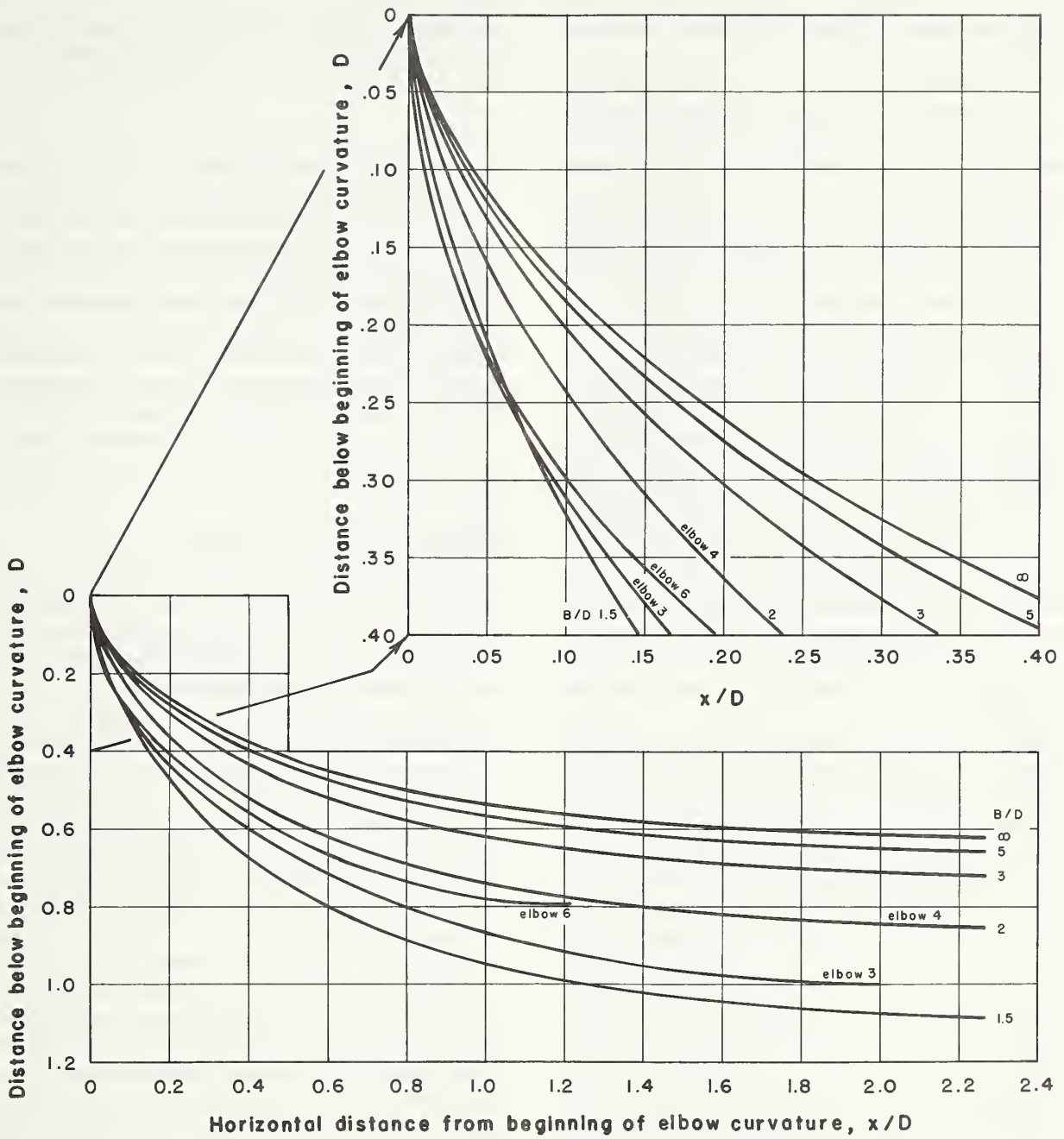

Figure XVI-15.—Free streamline elbow profiles compared with recommended elliptical elbow 3 and double circle elbow 6.

The elliptical elbow proportions are:

Elbow	*Minor axis*	*Major axis*
1	D/2	3D/2
2	3D/4	5D/4
3	D	2D

See figure XVI-2 for a comparison of the elbow shapes.

Elbow 1 has a sharply curved entrance. This caused an abrupt reduction of the pressure just downstream of its entrance as shown in figure XVI-11(a). For all drop inlet lengths, minimum pressures occurred at $x/D = 0.036$, followed by an adverse pressure gradient along the remainder of the elbow. As the drop inlet length increased, the minimum pressure increased and the adversity of the pressure gradient decreased. This variation is caused by the

decreasing tendency for flow separation at the elbow entrance as the drop inlet becomes longer.

The elbow 1 profile was not considered satisfactory because of the severe adverse pressure gradient for all drop inlet lengths and the low or negative pressure coefficients near the elbow entrance.

Elbow 2 is D/4 greater in height and D/4 shorter than elbow 1; figure XVI-2 shows that the elbow 2 entrance curvature is less sharp than the elbow 1 curvature.

As shown in figure XVI-11(b), the reduction of the pressures downstream of the entrance to elbow 2 is less than is shown for elbow 1 in figure XVI-11(a). Also, the pressure coefficients for elbow 2 are always positive. Although the pressure gradients remained favorable or zero for the longer drop inlets, for the 1.5D-long drop inlet the pressure reached a relative minimum at $x/D = 0.09$ followed by an adverse pressure gradient. At $x/D = 0.75$ the pressures fell to another relative minimum and the pressure gradient became adverse to the end of the elbow for all drop inlet lengths.

The pressure distribution for elbow 2 is not satisfactory.

Elbow 3 is D/4 greater in height and 3D/4 greater in length than elbow 2. Figure XVI-2 shows that elbow 3 has the least curvature and longest length of the elliptical elbows tested.

As shown in figure XVI-11(c), for the air tests elbow 3 had positive pressure coefficients for all inlet lengths and favorable gradients for all lengths except for a minor adversity between $x/D = 0.17$ and 0.35 for the 1.5D-long drop inlet. The water test results show slightly lower pressures for all drop inlet lengths and a slightly greater adversity for the 1.5D- and 2D-long drop inlets.

The pressure coefficients for elbow 3 when used in combination with transitions B through G shown in figures XVI-12(a)-(f) are close to those shown in figure XVI-11(c). This means that (1) the consistency of the results for elbow 3 is good and (2) the transition geometry has little effect on the elbow pressures.

The pressure characteristics of elbow 3, shown in figures XVI-11(c) and XVI-12, are better than those of free streamline elbow 4, shown in figures XVI-11(d) and XVI-13(a). This may be because the elbow 3 profile approaches that of the free streamline profile for the 1.5D-long drop inlet shown in figure XVI-15. Therefore, the elbow 3 profile is satisfactory for use between drop inlets and transitions from a semisquare-semicircular section to a circular section conduit.

As the inlet to a square barrel, elbow 3 does not perform as well as with the circular barrel. As shown in figure XVI-14(a), the pressure gradient is adverse between $x/D = 0.17$ and 0.60 for the 1.5D- and 2D-long drop inlets, and again adverse at the barrel entrance for all drop inlet lengths. Also, for all drop inlet lenghts the pressure coefficients approximate zero for the downstream one-third of the elbow. However, without the transition the entire reduction of flow area occurs along the elbow so the hydraulic gradeline at the elbow exit is lower than with a transition, thereby depressing the pressure coefficients along the elbow.

Double circle elbows 5 and 6

The double circle elbow 5, comprised of two 45-degree arcs of radii D/2 and 1D, was originally proposed by the SCS. The downstream arc of double circle elbow 6 was increased to 3D/2 to improve the elbow performance.

As shown in figure XVI-11(e), the pressures decreased rapidly downstream of the entrance to elbow 5. There is an adverse gradient between $x/D = 0.12$ and 0.34 for the 1.5D- and 2D-long drop inlets. At $x/D = 0.5$, the pressures decreased to a relative minimum close to zero. Beyond $x/D = 0.5$ there is a significant adverse gradient to the end of the elbow for all lengths of drop inlet.

Because the pressure distribution for elbow 5 was unsatisfactory, the radius of the downstream arc was increased to 3D/2 to form double circle elbow 6. The pressure coefficients along elbow 6 are shown in figures XVI-11(f) and XVI-13(b). Comparing the pressure coefficients for elbows 6 and 5 shows that along the upstream arc of elbow 6 ($x/D < 0.15$) the pressure coefficients are significantly higher than those for elbow 5. This is because the elbow entrance is larger and the velocity and velocity head lower because of the increased vertical height of the elbow 6 downstream arc. However, for the 1.5D- and 2D-long drop inlets, a relative minimum pressure occurs at $x/D = 0.07$, followed by adverse pressure gradients to $x/D = 0.31$. As for elbow 5, the pressures decreased again to a relative minimum well

above zero at x/D = 0.96, beyond which there was an adverse gradient to the end of the elbow for all lengths of drop inlet. The water test results for elbow 6, as for elbow 3, indicate slightly lower pressures.

The performance of elbow 6 when used with a transition as the entrance to a circular barrel is probably satisfactory despite the adverse pressure gradient regions.

Elbow 6 was tested with a flat invert and the square barrel. As shown in figure XVI-14(b), the pressure coefficients are significantly reduced from their values with the circular barrel. Minimum pressure coefficients down to −0.25 and severe adverse pressure gradients will limit the application of this elbow profile when the barrel is square.

Conclusions

Based on minimum average pressure coefficients and pressure gradients, elliptical elbow 3 and double circle elbow 6 are the best shapes tested.

With a semicylindrical invert, 2**D**-long elbow 3 consistently maintained the highest average pressure coefficients and had an adverse pressure gradient only with the 1.5**D**-long drop inlet. 1.21**D**-long elbow 6 is shorter but hydraulically less satisfactory than elbow 3 because of its lower pressure coefficients and minor to moderate adverse pressure gradients, but it is adequate. Elbow 4 also had a desirable pressure distribution but its length becomes almost 3**D** when the profile is extended to the one percent barrel slope commonly used with the two-way drop inlet spillway for which this type of entrance is needed.

With a flat invert and square barrel, elbows 3 and 6 had lower minimum pressures and more severe adverse pressure gradients. However, no attempt was made to improve the performance of these elbows because the flat invert-square barrel tests were made only to evaluate the elbow shapes developed for circular barrels and to provide some criteria for use with a rectangular barrel.

Transition Evaluation

The minimum pressure in a closed conduit transition generally occurs downstream of an adverse change in boundary alignment (a wall deviation away from the flow). Such a change in the boundary may be located some place other than on the crown of the transition. Therefore, presented in addition to the crown and invert pressure coefficients are the minimum average pressure coefficients and their locations.

Conical transitions A and B

The pressure coefficients for the 2**D**-long conical transition A-elbow 3 combination are given in figure XVI-11(c) and for the 1**D**-long conical transition B-elbow 3 combination in figure XVI-12(a). For both transitions the crown pressure coefficients and gradients are similar and satisfactory. However, the minimum pressures occur in the barrel 45° above the horizontal and 0.05**D** downstream from the end of the transition. For the 2**D**-long transition A, the adverse angle between the conical surface and the barrel wall is small (5.9°), the minimum coefficients approach zero as the drop inlet length increases, and there is an adverse gradient into the barrel. For the 1**D**-long transition B the adverse angle at the junction with the barrel is greater (11.7°), the pressure coefficient decreased to about −0.2 (a minimum of −0.25 for the 5**D**-long drop inlet), and there is a severe adverse pressure gradient near the barrel entrance.

As shown in figures XVI-11(a)-(f), similar pressure coefficients were obtained for transition A in combination with each of the six elbows. This indicates that the elbow has little, if any, effect on the transition pressures.

The results show that the 2**D**-long conical transition A is satisfactory but that the 1**D**-long conical transition B is too short.

Warped transitions

The warped surfaces in the upper corners of the transitions are circumferentially tangent to the barrel, so abrupt changes in wall alignment are avoided. However, the warped surfaces bend away from the flow (adverse wall curvature), causing regions of locally reduced pressure in the transition.

Warped transitions C, D and E are 1**D** long, and they are defined by cutting various profiles in the upper half of the pipe as viewed from the side and extending successive transverse tangents from the profile to the horizontal plane through the crown of the pipe. The transition shapes are illustrated in figures XVI-4(a)-(c).

The pressure coefficients for transitions C, D and E are plotted in figures XVI-12(b)-(d). The

crown pressure coefficients were measured 0.35**D** downstream of the transition entrance. When compared with transition C, the pressure coefficient there for transition D was slightly higher while transition E had a lower entrance pressure coefficient. The pressure coefficients near the exits are nearly the same for all three transitions. Located as described in figure XVI-12 legends, the minimum pressure coefficients approached zero as the drop inlet lengthened for transitions C and E, and the adverse pressure gradient was mild. For transition D with the 5**D**-long drop inlet the minimum pressure coefficient decreased to -0.04, causing a significant adverse pressure gradient.

Warped transitions F and G are defined by specifying the shape of their plane, horizontal, triangular tops, and by extending successive tangents from the sides of the top to the barrel circumference. The tangents form a warped surface on either side of the transition. These transitions are illustrated in figures XVI-4(c) and (d). Transition F is 1**D** long and transition G **D**/2 long.

The pressure coefficients for the transition F-elbow 3 combination are plotted in figure XVI-12(e) and the transition F-elbows 4 and 6 combinations in figures XVI-13(a) and (b). The air test crown pressure coefficients for transition F with each elbow combination are nearly the same and indicate a favorable pressure gradient along the transition. The minimum pressure coefficients decreased to zero as the drop inlet length increased to 5**D**, producing a mild adverse pressure gradient toward the transition exit.

As shown in figures XVI-12(e) and XVI-13(b), some of the water test results for transition F differ somewhat from the air test results. With elbow 3 both the crown and minimum pressure coefficients at 0.70**D** downstream of the transition entrance range from 0.08 to 0.11 below the corresponding air test results. At 0.05**D** downstream of the transition the water test coefficients are 0.05 below the corresponding air test values. With elbow 6 the respective water test pressure coefficients are 0.05 to 0.08 and 0.03 lower than the corresponding air test coefficients.

The cause of the differences between the air and water tests has not been determined. Because the differences are confined to two piezometer locations, they may be due to slight differences in the geometry of the air and the water models of transition F. Because of the uncertainty of which results are correct, the lower water test results should be used for design purposes.

For the water tests the minimum pressure coefficient was -0.08 for the 5**D**-long drop inlet, and the pressure gradient between 0.70**D** downstream of the transition entrance and 0.05**D** downstream of the transition exit was adverse.

Transition G has the same geometry as transition F, but it is **D**/2 long. The pressure coefficients for the transition G-elbow 3 combination are given in figure XVI-12(f). The pressure coefficients along the crown are positive, similar to those for transition F, and the crown gradient is satisfactory. However, with the rapid reduction of the flow area, the minimum pressure coefficients at 0.35**D** downstream of the transition entrance decreased to -0.25 for the 5**D**-long drop inlet and there was a severe adverse gradient into the conduit entrance.

Transition G was considered to be too short.

Conclusions

Considering geometry as well as the pressure characteristics, the 2**D**-long conical transition A and the 1**D**-long warped transition F were selected as the best transitions. The pressure coefficients and gradients for warped transitions C and E are also satisfactory.

Transition A had high pressure coefficients and favorable pressure gradients throughout with all drop inlet lengths for both the air and the water tests. However, the break in the wall alignment at 45° on both sides of the crown at the transition exit reduced the pressure coefficients to zero and created a minor adverse pressure gradient.

Transition F was selected because the air test pressure coefficients were adequate, its length was one-half that of transition A, and its geometry was more easily defined than those of the other type of warped transition. The minimum water test pressure coefficients were lower, increasing the adversity of the pressure gradient, but these factors can be considered during the design of closed conduit spillways.

The short versions of conical transition B and triangular-topped, warped transition G were unsatisfactory because of low pressure coefficients and severe adverse pressure gradients.

Of the other warped transitions, transitions C

and E had satisfactory pressure distributions and minor adverse pressure gradients, while transition D had a significant adverse pressure gradient, but all three have a geometry that may be difficult to form in concrete.

Minimum Average Pressure Coefficients

The minimum pressures determine the cavitation potential. The minimum pressure is the algebraic sum of the minimum average pressure and the pressure fluctuation about the average. In this section the minimum average pressure coefficients for elbows 3 and 6 and transitions A and F will be discussed and compared to those of other inlet geometries. Pressure fluctuations about the minimum average pressures will be discussed in a following section.

The elbow and transition evaluations indicated that the minimum pressure coefficient for each geometry varied with the drop inlet length, so an analysis was made to relate them. There were also differences between the air and water test results. In both cases the lowest minimum coefficients obtained from all tests on each geometry were used for analysis. From the resulting relationships the minimum average pressure can be readily determined for any geometrically similar barrel entrance.

Elbows 3 and 6 with circular barrel

Figure XVI-16 illustrates, for each drop inlet length, the minimum average pressure coefficients for elbows 3 and 6 with transitions A and F for both the water and the air tests and the circular conduit.

The minimum pressure coefficients for elbow 3 shown at $x/D = 1.90$ in figures XVI-11(c) and XVI-12(e) are shown in figure XVI-16(a) to be relatively independent of the drop inlet length. The minimum average pressure coefficient for elbow 3 used with transitions A and F as the entrance to a circular barrel is

$$\frac{h_n}{h_{vp}} 0.22 \qquad \text{(XVI-2)}$$

For elbow 6 the minimum pressure coefficients, which occurred at $x/D = 0.96$ as shown in figures XVI-11(f) and XVI-13(b), are shown in figure XVI-16(b) to vary with the drop inlet length. The minimum average pressure coefficients for elbow 6 used with transitions A and F as the entrance to a circular barrel are

$$\frac{h_n}{h_{vp}} = 0.04 \left\langle 2.75 - \frac{B}{D} \right\rangle + 0.08 \qquad \text{(XVI-3)}$$

in which the term in pointed brackets is zero when $B/D > 2.75$.

Transitions A and F

The minimum average pressure coefficients for transitions A and F are plotted in figure XVI-17. The plots show that the minimum average pressure coefficient varies inversely as a function of the drop inlet length.

For transition A the minimum average pressure coefficients shown in figure XVI-17(a) occurred 0.05**D** downstream of the transition exit as shown in figures XVI-11(c) and XVI-11(f). As shown in figure XVI-17(a), although the minimum average pressure coefficients are constant at $h_n/h_{vp} = 0.00$ for the longer drop inlets, an exponential relationship provides a better fit to the minimum coefficients for all lengths of drop inlet. Therefore, the minimum average pressure coefficients for transition A are

$$\frac{h_n}{h_{vp}} = \frac{0.14}{(B/D)^{0.3}} - 0.1 \qquad \text{(XVI-4)}$$

For transition F the minimum average pressure coefficients shown in figure XVI-17(b) occurred 0.7**D** downstream of the transition entrance as shown in figures XVI-12(e) and XVI-13(b). The minimum average pressure coefficients for transition F are given by the exponential relationship

$$\frac{h_n}{h_{vp}} = \frac{0.18}{(B/D)^{1.30}} - 0.1 \qquad \text{(XVI-5)}$$

Elbows 3 and 6 with square barrel

The minimum pressure coefficients for elbows 3 and 6 were lower with the square barrel and flat elbow inverts than with the circular barrel and semicylindrical inverts.

For elbow 3 the minimum pressure coefficients shown in figure XVI-18(a) occurred at $x/D = 1.90$ as shown in figure XVI-14(a). The coefficients became slightly negative as the drop inlet length increased. The minimum average pressure coefficients for elbow 3 with a square barrel are

$$\frac{h_n}{h_{vp}} = -0.01 \frac{B}{D} + 0.02 \qquad \text{(XVI-6)}$$

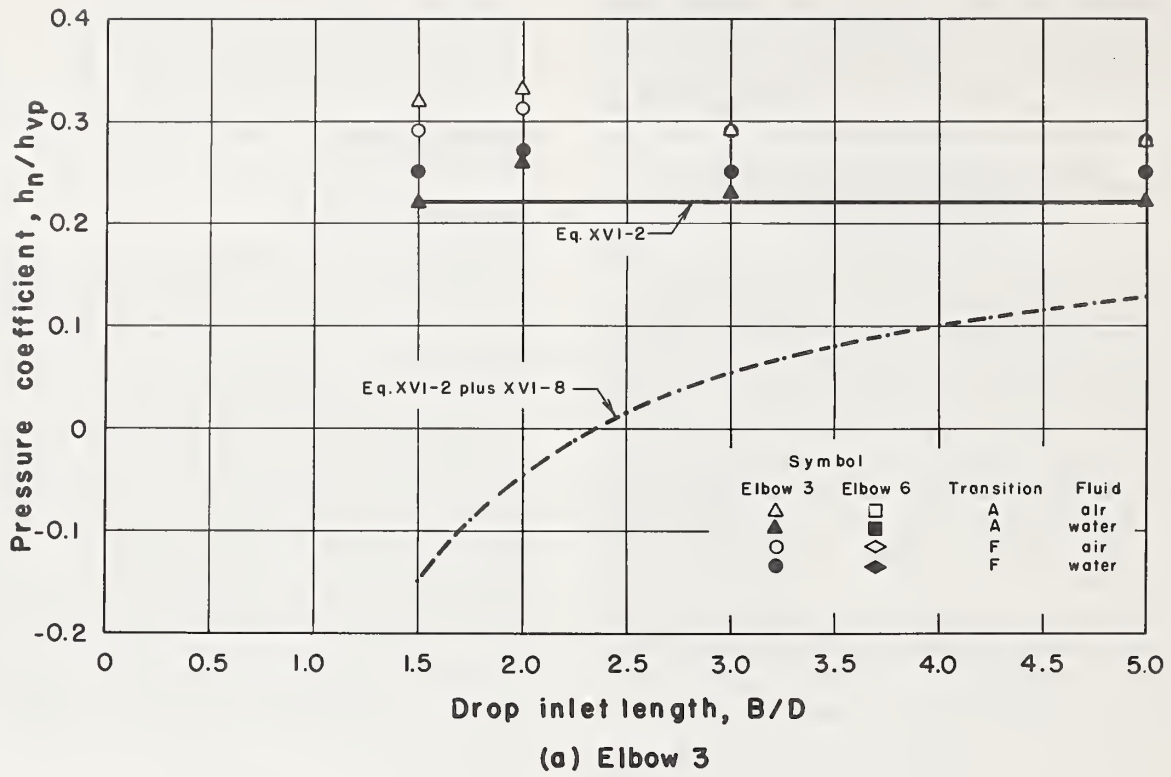

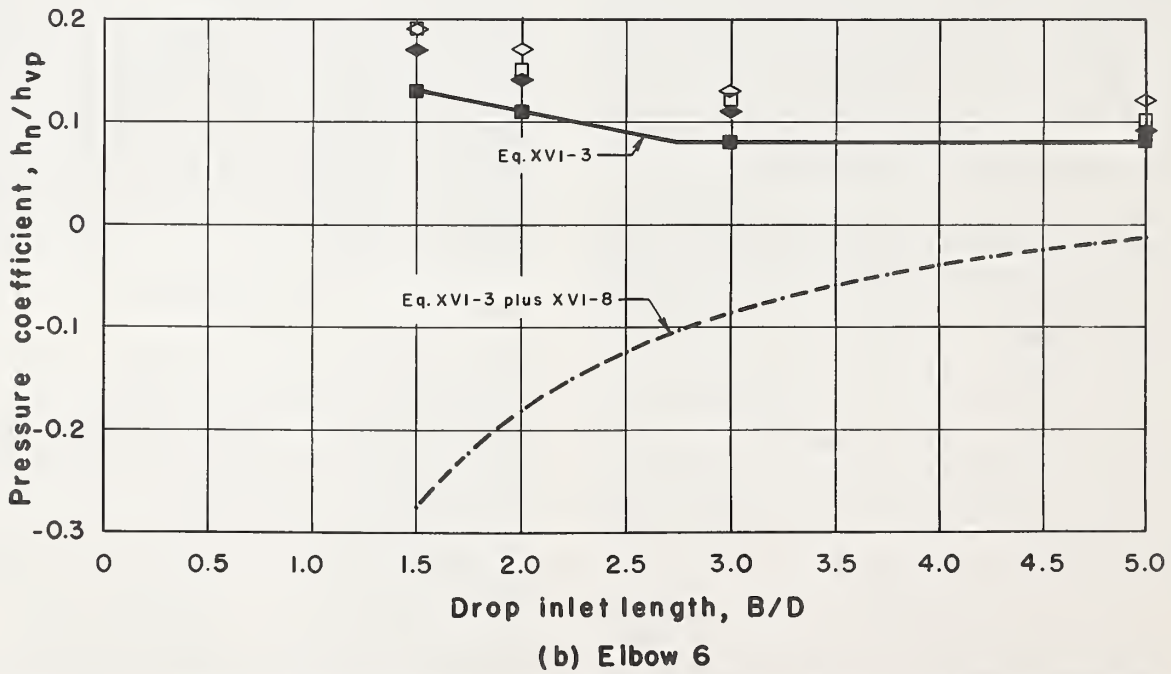

Figure XVI-16.—Minimum average and instantaneous pressure coefficients for elbows 3 and 6 with circular barrel.

For elbow 6 the minimum average pressure coefficients shown in figure XVI-18(b) occurred at $x/D = 0.96$ as shown in figure XVI-14(b) and were negative for all lengths of drop inlet. The minimum average pressure coefficients for elbow 6 with the square barrel are

$$\frac{h_n}{h_{vp}} = \frac{0.25}{B/D} - 0.30 \qquad \text{(XVI-7)}$$

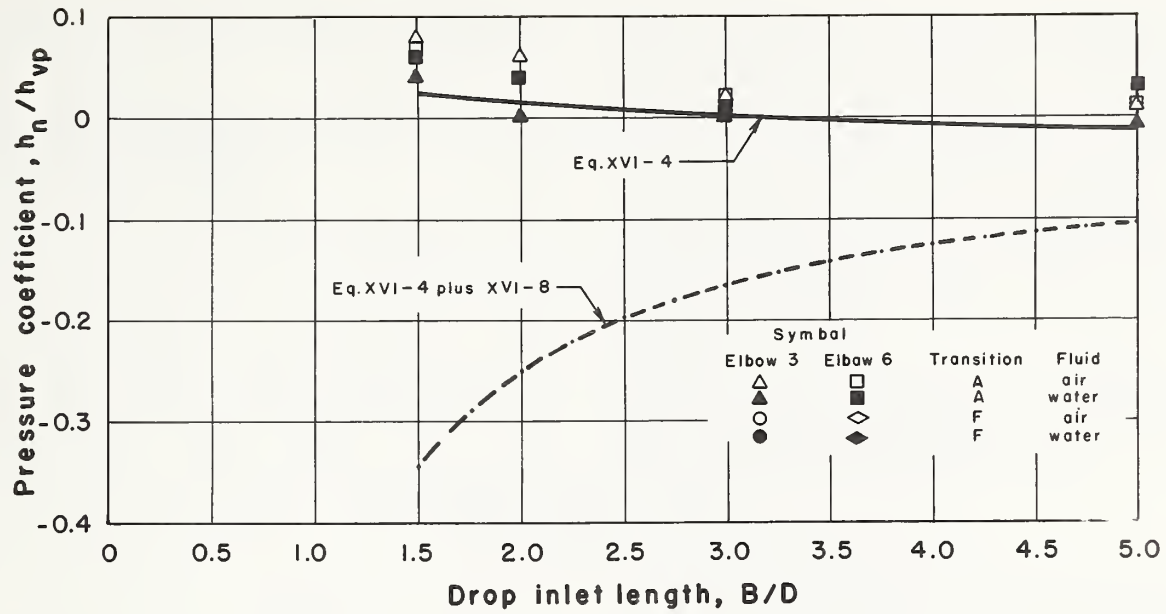

(a) Transition A

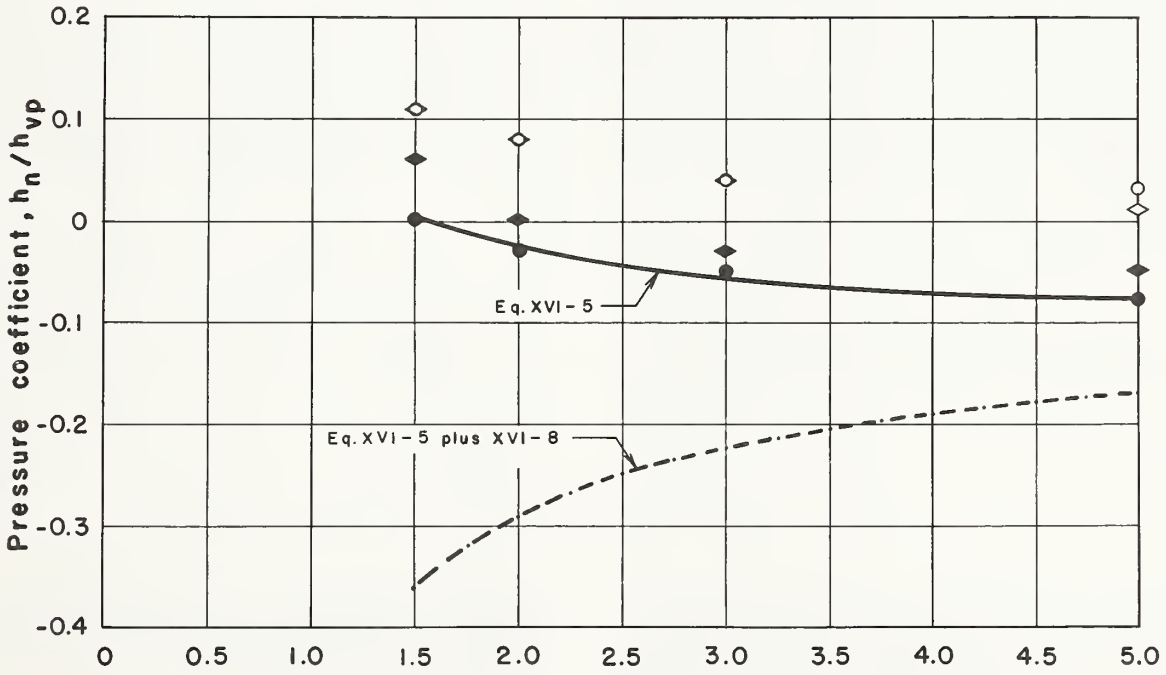

(b) Transition F

Figure XVI-17.—Minimum average and instantaneous pressure coefficients for transitions A and F.

Effect of elbow-transition on the minimum average pressure coefficient

An objective of the elbow and transition was to streamline the inlet to the spillway barrel to reduce the cavitation potential. Comparisons of the minimum average pressure coefficients for several inlet shapes used between 2**D**-long drop

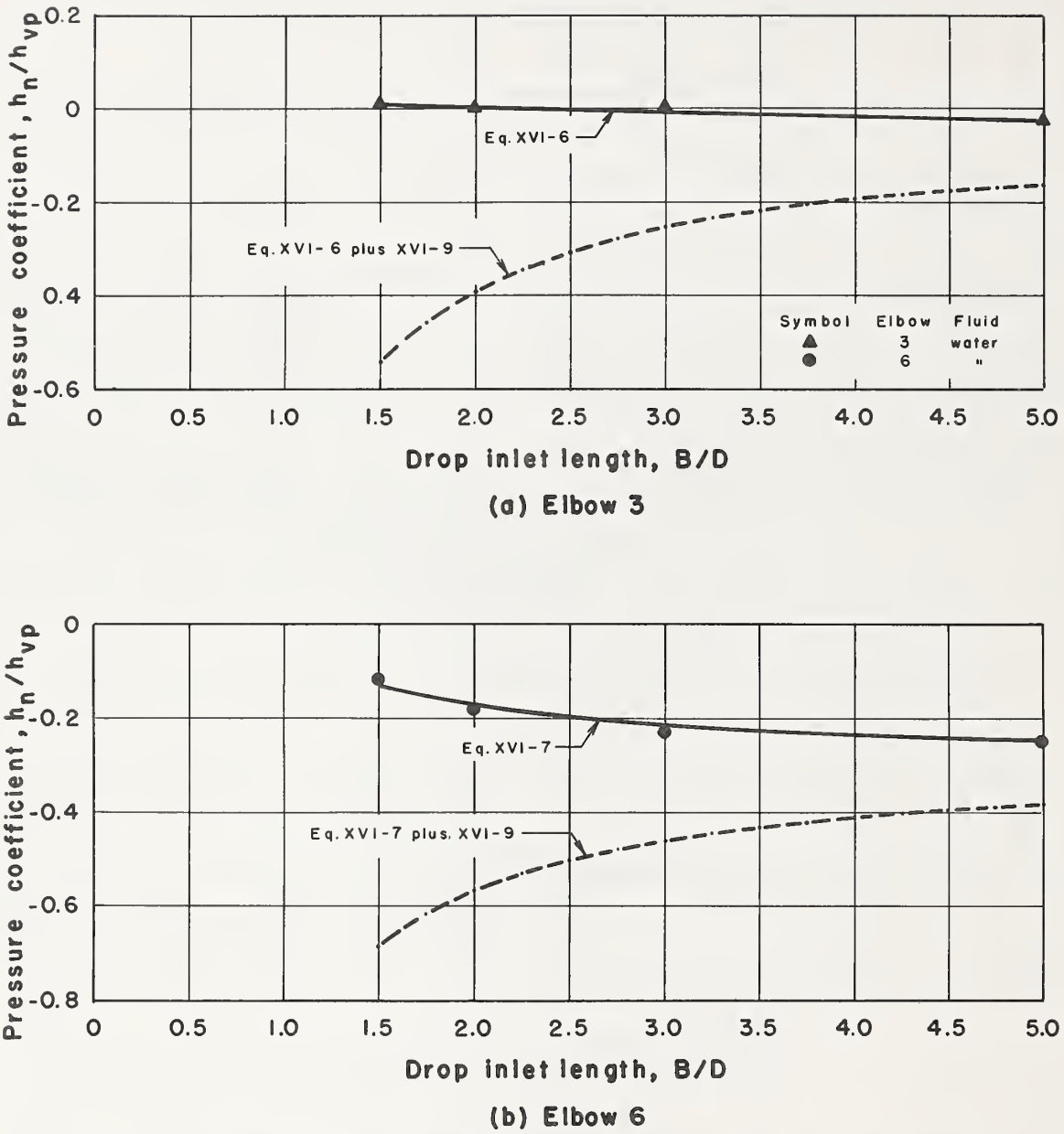

Figure XVI-18.—Minimum average pressure coefficients for elbows 3 and 6 with square barrel.

inlets and a barrel with zero slope are given in table XVI-5. The 2**D**-long drop inlet was selected for comparison because test results were available for the greatest variety of inlet geometries.

Table XVI-5 shows the square-edged entrances cause a large reduction in the entrance pressure. This pressure reduction is due to the abrupt change in boundary alignment above the barrel midheight, which causes separation of the flow as the jet enters the barrel. For both drop inlets with the square-edged barrel entrance, the hydraulic gradeline was about $1.2h_{vp}$ below the friction gradeline at 0.5**D** downstream of the barrel entrance.

The Swarthmore elbow-transition inlet is streamlined so it reduced the tendency for flow separation. For the Swarthmore inlet the hydraulic gradeline was $0.14h_{vp}$ below the friction gradeline.

When elbow 3 or 6 is combined with transition A or F the hydraulic gradeline is a minimum of $0.01h_{vp}$ above the friction gradeline for transi-

TABLE XVI-5.—*Minimum average pressure coefficients for several two-way drop inlet barrel entrances*

Entrance	Location[1]	h_n/h_{vp}
Flat drop inlet invert with square-edged circular barrel entrance[2]	0.5D	−1.21
Semicylindrical drop inlet invert with square-edged circular barrel entrance[3]	.5D	−1.17
Swarthmore elbow and transition[4]	.0D	− .14
Elbow 3 or 6 and transition A	.05D	+ .01
Elbow 3 or 6 and transition F	− .3D	− .03
Elbow 3 with square barrel	− .1D	.00
Elbow 6 with square barrel	− .25D	− .18

[1] Location with respect to barrel entrance, positive toward downstream.

[2] Part XII, figure XII-1, entrance a.

[3] Part XVII (In press).

[4] Value determined by analysis of data presented in reference in footnote 5, page 2.

tion A and a maximum of $0.03h_{vp}$ below the friction gradeline for transition F. When the barrel is square, the lowest pressure for elbow 3 coincides with the friction gradeline and the minimum pressure for elbow 6 falls well below ($-0.18h_{vp}$) the friction gradeline.

The comparisons presented in table XVI-5 show that the elbows and transitions developed as a result of this study have the least cavitation potential of the inlets compared.

Pressure Fluctuations

The flow of water in conduits is usually turbulent and pressure fluctuations about the average pressure are expected. Additional turbulence in the drop inlet and in the barrel entrance causes larger pressure fluctuations. Negative pressure fluctuations increase the possibility of cavitation and cavitation-caused damage; as stated under the heading "Pressures" (page 12), negative pressure fluctuations can be large enough to initiate cavitation damage even though the average pressure is positive. To evaluate the effect of the negative pressure fluctuations on the cavitation potential, the pressure fluctuations at the locations of the minimum pressures identified in the previous section were recorded and analyzed. Although a spectral analysis was not practical, the maximum fluctuations were estimated from the oscillograph charts.

The maximum pressure fluctuations from the average pressure were determined for each test of the four combinations of elbows 3 and 6 and transitions A and F with the circular barrel and elbows 3 and 6 with the square barrel. The maximum pressure fluctuation used in the analyses is the average of the single maximum pressure fluctuation observed during each test run. Up to 30 runs were made on each elbow-transition combination. The maximum pressure fluctuations, Δh_n, were expressed in terms of the barrel velocity head, Δh_{vp}, to make them dimensionless and directly addable to the average pressure coefficients.

The dimensionless pressure fluctuation coefficients, $\Delta h_n/h_{vp}$, were analyzed to determine the effect of Reynolds number and drop inlet length on the fluctuations for each geometry.

Effect of the Reynolds number

Inspection of the test results showed that the maximum pressure fluctuation coefficients at each piezometer location for each drop inlet length and elbow-transition combination were similar for all tests. The maximum pressure fluctuation coefficients seldom varied more than 30 percent from their respective means. This agreement is sufficient evidence, in view of the random nature of turbulence and the manual analysis of the fluctuation data, to conclude that the pressure fluctuation coefficient is independent of the discharge or Reynolds number. Therefore, the average maximum fluctuation coefficients given in table XVI-6 were used for all subsequent analyses.

The actual pressure fluctuations for the square barrel were about the same as those for the circular barrel, but the average pressure fluctuation coefficients for the square barrel are higher than those for the circular barrel because the velocity head in the square barrel—the denominator in the $\Delta h_n/h_{vp}$ ratio—is $(\pi/4)^2 = 0.617$ times that of the circular barrel; if the fluctuation coefficients in table XVI-6 for the square barrel are multiplied by $(\pi/4)^2$ the values fall within the range of values in table XVI-6 for the circular barrel.

Effect of elbow-transition geometry

A comparison of the pressure fluctuation coefficients listed in table XVI-6 for each elbow-transition-drop inlet combination shows that the elbow and transition coefficients for each combination are, within the degree of precision inherent in the analyses, probably identical.

TABLE XVI-6.—*Average maximum pressure fluctuation coefficients,* $\Delta h_n/h_{vp}$

Drop inlet length	Circular barrel Elbow: Transition combination				Square barrel Elbow	
	3[1] : A[2]	3[1] : F[3]	6[4] : A[2]	6[4] : F[3]	3[1]	6[4]
1.5D	−0.26 : −0.28 + .25 : + .22	−0.23 : −0.28 + .23 : + .22	−0.31 −0.36 : −0.28 + .29 + .19 : + .20	−0.37 −0.40 : −0.33 + .32 + .20 : + .31	−0.44 + .37	−0.58 −0.56 + .48 + .32
2D	− .18 : − .18 + .17 : + .14	− .16 : − .18 + .16 : + .16	− .24 − .18 : − .20 + .20 + .11 : + .14	− .24 − .26 : − .21 + .24 + .17 : + .19	− .30 + .29	− .34 − .37 + .38 + .24
3D	− .11 : − .10 + .13 : + .09	− .10 : − .08 + .11 : + .08	− .14 − .08 : − .08 + .09 + .04 : + .05	− .13 − .12 : − .09 + .15 + .10 : + .10	− .18 + .18	− .23 − .17 + .23 + .14
5D	− .06 : − .06 + .06 : + .06	− .06 : − .06 + .07 : + .06	− .06 − .10 : − .05 + .05 + .08 : + .04	− .08 − .09 : − .06 + .09 + .08 : + .09	− .11 + .11	− .14 − .11 + .14 + .08

[1] Located at x/D = 1.90.
[2] Located 0.05D downstream of transition exit.
[3] Located 0.7D downstream of transition entrance.
[4] Located at x/D = 0.10 and 0.96, respectively.

This indicates that the pressure fluctuations are not damped appreciably between the points at which the pressure fluctuations were recorded.

A comparison of the pressure fluctuation coefficients for each drop inlet length shows that the variation with elbow-transition geometry is also within the limits of precision imposed by the experimental methods.

The results of these analyses indicate that the effect of the elbow-transition geometry on the pressure fluctuation coefficients is minimal.

Effect of drop inlet length

Table XVI-6 shows that the pressure fluctuation coefficients decrease as the drop inlet length increases so the pressure fluctuation coefficient, like the average pressure coefficient, is a function of the drop inlet length.

The pressure fluctuation coefficients become increasingly significant as the drop inlet length decreases: As a function of the barrel velocity head for the circular and square barrels, respectively, they increase from 5 and 11 percent for the 5D-long drop inlets to 40 and 58 percent for the 1.5D-long drop inlets.

The maximum negative pressure fluctuation coefficients listed in table XVI-6 are listed in table XVI-7. These values are used to derive the relationship between the drop inlet length and the maximum negative pressure fluctuation from the average pressure. The resulting equations are:

for the circular barrel,

$$\frac{\Delta h_n}{h_{vp}} = -\frac{0.57}{(B/D)^{1.17}} \qquad \text{(XVI-8)}$$

and for the square barrel,

$$\frac{\Delta h_n}{h_{vp}} = -\frac{0.92}{(B/D)^{1.17}} \qquad \text{(XVI-9)}$$

Computed values of h_n/h_{vp} and differences from the observed values are given in table XVI-7. The equations and the maximum negative pressure fluctuation coefficients agree within 4 percent of a velocity head.

Instantaneous Minimum Pressure Coefficients

As stated earlier, the pressure fluctuations momentarily reduce the minimum average pressure coefficients. Because both the average

TABLE XVI-7.—*Maximum negative pressure fluctuation coefficients,* $\Delta h_n/h_{vp}$

Drop inlet length	Circular conduit			Square conduit		
	Observed	Computed	Difference	Observed	Computed	Difference
1.5D	−0.40	−0.36	+0.04	−0.58	−0.58	0.00
2D	− .26	− .25	+ .01	− .37	− .41	− .04
3D	− .14	− .16	− .02	− .23	− .26	− .03
5D	− .10	− .09	+ .01	− .14	− .14	.00

pressure coefficient and the fluctuation pressure coefficient are expressed in terms of the barrel velocity head, they can be added to determine the instantaneous minimum pressure coefficient.

The instantaneous average minimum pressure coefficients have been computed for elbows 3 and 6 and transitions A and F and are shown as dashed lines in figures XVI-16, XVI-17, and XVI-18. The maximum fluctuations are large, particularly for the shorter drop inlet lengths, so that the momentary minimum pressures are much lower than the average pressures.

If the momentary low pressures reach the vapor pressure and occur so frequently that the aggregate time in the cavitation range is large, cavitation damage can be expected even though the average pressure will not cause cavitation.

ENERGY LOSSES

The energy losses were determined for each elbow and transition combination. The entrance energy loss coefficient K_e is the total energy head lost between the reservoir pool level and the barrel, including any losses in the barrel caused by the entrance, h_e divided by the velocity head in the barrel $V_p^2/2g$. In equation form

$$K_e = \frac{h_e}{V_p^2/2g} \qquad \text{(XVI-10)}$$

The entrance energy loss coefficient K_e was divided into a crest energy loss coefficient K_c and a barrel entrance energy loss coefficient K_t. Division of the entrance losses in this manner allows the designer to select the crest and barrel entrance geometries independently and add their loss coefficients to get the total entrance energy loss coefficient.

The crest energy loss coefficient K_c is the energy loss between the headpool and the midheight of the drop inlet in terms of the drop inlet velocity head or

$$K_c = \frac{h_c}{V_r^2/2g} \qquad \text{(XVI-11)}$$

where h_c is the loss in head between the headpool surface and the midheight of the drop inlet, $V_r = Q/A_r$ is the average velocity in the drop inlet, Q is the rate of flow, A_r is the cross-sectional area of the drop inlet, and g is the acceleration of gravity.

The barrel entrance energy loss coefficient K_t is defined as the head loss between the midheight of the drop inlet and the barrel entrance plus the loss in the barrel caused by the entrance divided by the barrel velocity head or

$$K_t = \frac{h_t}{V_p^2/2g} \qquad \text{(XVI-12)}$$

where $V_p = Q/A_p$ is the average velocity in the barrel, A_p is the area of the barrel cross section, and h_t is the actual head loss—the difference between the energy head at the drop inlet midheight and the energy head at the barrel entrance determined by extending the barrel friction gradeline to the barrel entrance. The energy head at the barrel entrance is defined in this manner to separate the turbulence losses caused by the entrance from the friction loss in the barrel so that K_t is independent of other losses in the spillway. This makes K_t indicative of the energy efficiency of the barrel entrance geometry.

The experimental data used in the analysis are summarized in table XVI-8. In addition, the observed coefficients corrected for mislocation of the drop inlet midheight piezometer, the computed entrance energy loss coefficients, and comparisons with the experimental values are also listed in table XVI-8.

The energy loss coefficients and the parameters that affect them will be discussed and evaluated in following sections.

Barrel Entrance Energy Loss Coefficient Correction

The crest head loss h_c and the barrel entrance head loss h_t were determined from a single piezometer located at the midheight of the drop inlet. In all previous two-way drop inlet tests at the St. Anthony Falls Hydraulic Laboratory this midheight piezometer was located 1**D** upstream of the downstream endwall of the drop inlet. However, for this study the piezometer was inadvertently placed 0.5**D** upstream of the downstream endwall so the crest and barrel entrance energy loss coefficients were not compatible with those from earlier studies of the crest and barrel entrance losses for the two-way drop inlet.

TABLE XVI-8.—*Summary of energy loss coefficients*

Air tests (B-): D = 0.249 ft

Water tests (W-): D = 0.1875 ft

Series	B/D	Elbow	Transition	K_c	K_t				K_t'	ΔK_t	K_e		
				Computed	Observed	Corrected	Computed	Difference			Observed	Computed	Difference
						Circular barrel							
B-100	5	1	A	2.48	0.11	0.136	0.102	−0.03	0.14	0.03	0.20	0.163	−0.04
B-101	3	1	A	1.67	.10	.126	.133	.01	.125	.025	.24	.248	.01
B-102	2	1	A	1.48	.14	.166	.187	.02	.16	.02	.39	.415	.02
B-103	1.5	1	A	1.42	.21	.236	.257	.02	.23	.02	.62	.646	.03
B-104	5	5	A	2.48	.07	(1)	.102	(1)	.09	.02	.15	(1)	(1)
B-105	3	5	A	1.67	.07	(1)	.133	(1)	.085	.015	.20	(1)	(1)
B-106	2	5	A	1.48	.08	(1)	.187	(1)	.07	−.01	.30	(1)	(1)
B-107	1.5	5	A	1.42	.17	(1)	.257	(1)	.16	−.01	.55	(1)	(1)
B-108	5	2	A	2.48	.09	.116	.102	−.01	.12	.03	.18	.163	−.02
B-109	3	2	A	1.67	.12	.146	.133	.01	.145	.025	.26	.248	−.01
B-110	2	2	A	1.48	.16	.186	.187	.00	.19	.03	.42	.415	.00
B-111	1.5	2	A	1.42	.24	.266	.257	−.01	.27	.03	.66	.646	−.01
B-112	5	3	A	2.48	.07	.096	.102	.01	.11	.04	.17	.163	−.01
B-113	3	3	A	1.67	.12	.146	.133	−.01	.155	.035	.27	.248	−.02
B-114	2	3	A	1.48	.19	.216	.187	−.03	.23	.04	.46	.415	−.04
B-115	1.5	3	A	1.42	.25	.276	.257	−.02	.29	.04	.68	.646	−.03
B-116	5	3	B	2.48	.06	.086	.102	−.02	.10	.04	.16	.163	.00
B-117	3	3	B	1.67	.10	.126	.133	.01	.135	.035	.25	.248	.00
B-118	2	3	B	1.48	.15	.176	.187	.01	.19	.04	.42	.415	.00
B-119	1.5	3	B	1.42	.21	.236	.257	.02	.25	.04	.64	.646	.01
B-120	5	3	C	2.48	.07	.096	.102	.01	.11	.04	.17	.163	−.01
B-121	3	3	C	1.67	.11	.136	.133	.00	.145	.035	.26	.248	−.01
B-122	2	3	C	1.48	.16	.186	.187	.00	.20	.04	.43	.415	−.02
B-123	1.5	3	C	1.42	.24	.266	.257	−.01	.28	.04	.67	.646	−.02
B-124	5	3	D	2.48	.09	.116	.102	−.01	.13	.04	.19	.163	−.03
B-125	3	3	D	1.67	.11	.136	.133	.00	.145	.035	.26	.248	−.01
B-126	2	3	D	1.48	.16	.186	.187	.00	.20	.04	.43	.415	−.02
B-127	1.5	3	D	1.42	.23	.256	.257	.00	.28	.05	.67	.646	−.02
B-128	5	3	E	2.48	.09	.116	.102	−.01	.13	.04	.19	.163	−.03
B-129	3	3	E	1.67	.10	.126	.133	.01	.135	.035	.25	.248	.00
B-130	2	3	E	1.48	.15	.176	.187	.01	.18	.03	.41	.415	.00
B-131	1.5	3	E	1.42	.22	.246	.257	.01	.25	.03	.64	.646	.01
B-132	5	6	A	2.48	.07	.096	.102	.01	.10	.03	.16	.163	.00
B-133	3	6	A	1.67	.10	.126	.133	.01	.125	.025	.24	.248	.01
B-134	2	6	A	1.48	.16	.186	.187	.00	.18	.02	.41	.415	.00
B-135	1.5	6	A	1.42	.23	.256	.257	.00	.25	.02	.64	.646	.01
B-136	5	3	F	2.48	.07	.096	.102	.01	.10	.03	.16	.163	.00
B-137	3	3	F	1.67	.11	.136	.133	.00	.155	.045	.27	.248	−.02
B-138	2	3	F	1.48	.16	.186	.187	.00	.19	.03	.42	.415	.00
B-139	1.5	3	F	1.42	.24	.266	.257	.00	.26	.02	.65	.646	.00
B-140	5	3	G	2.48	.08	.106	.102	.00	.11	.03	.17	.163	−.01
B-141	3	3	G	1.67	.11	.136	.133	.00	.135	.025	.25	.248	.00
B-142	2	3	G	1.48	.16	.186	.187	.00	.20	.04	.43	.415	−.02
B-143	1.5	3	G	1.42	.23	.256	.257	.00	.28	.05	.67	.646	−.02
B-144	5	4	A	2.48	.05	.076	.102	.03	.08	.03	.14	.163	.02
B-145	3	4	A	1.67	.11	.136	.133	.00	.145	.035	.26	.248	−.01
B-146	2	4	A	1.48	.16	.186	.187	.00	.19	.03	.42	.415	.00
B-147	1.5	4	A	1.42	.24	.266	.257	−.01	.28	.04	.67	.646	−.02
B-148	5	3	F	2.48	.08	.106	.102	.00	.12	.04	.18	.163	−.02
B-149	3	3	F	1.67	.12	.146	.133	−.01	.155	.035	.27	.248	−.02
B-150	2	3	F	1.48	.17	.196	.187	−.01	.21	.04	.44	.415	−.02
B-151	1.5	3	F	1.42	.23	.256	.257	.00	.28	.05	.67	.646	−.02

TABLE XVI-8.—*Summary of energy loss coefficients*—Continued
Air tests (B-): D = 0.249 ft
Water tests (W-): D = 0.1875 ft

Series	B/D	Elbow	Transition	K_c	K_t				K_t'	ΔK_t	K_e		
				Computed	Observed	Corrected	Computed	Difference			Observed	Computed	Difference
							Circular barrel						
B-152	5	3	F	2.48	.08	.106	.102	.00	.12	.04	.18	.163	– .02
B-153	3	3	F	1.67	.11	.136	.133	.00	.145	.035	.26	.248	– .01
B-154	2	3	F	1.48	.16	.186	.187	.00	.20	.04	.43	.415	– .02
B-155	1.5	3	F	1.42	.23	.256	.257	.00	.27	.04	.66	.646	– .01
B-156	5	6	F	2.48	.08	.106	.102	.00	.11	.03	.17	.163	– .01
B-157	3	6	F	1.67	.11	.136	.133	.00	.135	.025	.25	.248	.00
B-158	2	6	F	1.48	.16	.186	.187	.00	.18	.02	.41	.415	.00
B-159	1.5	6	F	1.42	.22	.246	.257	.01	.26	.04	.65	.646	.00
B-160	5	4	F	2.48	.08	.106	.102	.00	.11	.03	.17	.163	– .01
B-161	3	4	F	1.67	.10	.126	.133	.01	.125	.025	.24	.248	.01
B-162	2	4	F	1.48	.15	.176	.187	.01	.18	.03	.41	.415	.00
B-163	1.5	4	F	1.42	.22	.246	.257	.01	.25	.03	.64	.646	.01
W-622	5	3	A	2.52	.08	.106	.102	.00	.11	.03	.17	.164	– .01
W-623	3	3	A	1.72	.12	.146	.133	– .01	.13	.01	.25	.251	.00
W-624	2	3	A	1.52	.155	.181	.187	.01	.17	.015	.40	.421	.02
W-625	1.5	3	A	1.46	.22	.246	.257	.01	.21	– .01	.61	.657	.05
W-626	5	3	F	2.52	.07	.096	.102	.01	.09	.02	.15	.164	.01
W-627	3	3	F	1.72	.10	.126	.133	.01	.11	.01	.23	.251	.02
W-628	2	3	F	1.52	.17	.196	.187	.01	.18	.01	.41	.421	.01
W-629	1.5	3	F	1.46	.22	.246	.257	.01	.19	– .03	.59	.657	.07
W-630	5	6	F	2.52	.07	.096	.102	.01	.08	.01	.14	.164	.02
W-631	3	6	F	1.72	.09	.116	.133	.02	.09	.00	.21	.251	.04
W-632	2	6	F	1.52	.15	.176	.187	.01	.14	– .01	.37	.421	.05
W-633	1.5	6	F	1.46	.21	.236	.257	.02	.18	– .03	.58	.657	.08
W-634	5	6	A	2.52	.08	.106	.102	.00	.10	.02	.16	.164	.00
W-635	3	6	A	1.72	.10	.126	.133	.01	.11	.01	.23	.251	.02
W-636	2	6	A	1.52	.14	.166	.187	.02	.14	.00	.37	.421	.05
W-637	1.5	6	A	1.46	.20	.226	.257	.03	.17	– .03	.57	.657	.09
							Square barrel						
W-638	5	6	—	2.52	.07	.096	.102	.01	.10	.03	.20	.203	.00
W-639	3	6	—	1.72	.10	.126	.133	.01	.13	.03	.32	.324	.00
W-640	2	6	—	1.52	.19	.216	.187	– .03	.21	.02	.59	.567	– .02
W-641	1.5	6	—	1.46	.24	.266	.257	– .01	.22	– .02	.87	.906	.04
W-642	5	3	—	2.52	.07	.096	.102	.01	.10	.03	.20	.203	.00
W-643	2	3	—	1.52	.14	.166	.187	.02	.15	.01	.53	.567	.04
W-644	1.5	3	—	1.46	.25	.276	.257	– .02	.28	.03	.93	.906	– .02
W-645	3	3	—	1.72	.09	.116	.133	.02	.11	.02	.30	.324	.02

[1] Because of large deviations of observed K_t and K_e values from the overall mean values, air test data for elbow 5 and transition A (Series B-104 through B-107) were excluded from the energy loss analyses.

As explained in the following section, no use was made of the crest loss data obtained during this study. Therefore, the error in h_c caused by the mislocated drop inlet midheight piezometer was not corrected. However, the experimental barrel entrance energy loss coefficients were corrected by determining and applying the error caused by the midheight piezometer mislocation.

If equations XVI-10, XVI-11, and XVI-12 are solved for h_e, h_c, and h_t, respectively, the results are substituted into

$$h_e = h_c + h_t \qquad \text{(XVI-13)}$$

and both sides of the equation are divided by the barrel velocity head, $V_p^2/2g$, after simplifying the result is

$$K_e = K_c \left(\frac{V_r}{V_p} \right)^2 + K_t \qquad \text{(XVI-14)}$$

By continuity, this relationship can be expressed in terms of the area ratio as

$$K_e = K_c\left(\frac{A_p}{A_r}\right)^2 + K_t \qquad \text{(XVI-15)}$$

where $A_p/A_r = \pi/4(B/D)$ for the circular barrel and $1/(B/D)$ for the square barrel.

Because the entrance energy loss, h_e, is determined independently of the mislocated midheight piezometer, the experimental entrance energy loss coefficients K_e in table XVI-8 are valid for any midheight piezometer location and are compatible with the values of K_e obtained during earlier two-way drop inlet studies. So the experimental entrance energy loss coefficients K_e and the crest energy loss coefficients K_c, computed using equation XII-9, can be substituted into equation XVI-15 to obtain estimates of the barrel entrance energy loss coefficient

$$K_t' = K_{e,obs} - K_{c,comp}\left(\frac{A_p}{A_r}\right)^2 \qquad \text{(XVI-16)}$$

These estimated values are tabulated in table XVI-8 for each elbow-transition combination.

The experimental values of the barrel entrance energy loss coefficient were compared with the estimated values to estimate the error caused by the mislocation of the midheight piezometer. The resultant error or difference

$$\Delta K_t = K_t' - K_{t,obs} \qquad \text{(XVI-17)}$$

given for each geometry in table XVI-8 was quite constant for the air tests with an average value of 0.034, but for the water tests ranged from 0.03 to −0.03 with an average value of 0.007. Because the error was approximately constant for most of the tests, the overall average $\Delta K_t = 0.026$ was used to correct the experimental barrel entrance loss coefficient for each geometry as shown in table XVI-8.

Crest Energy Loss Coefficient[13]

Because the study reported here is on the elbow and transition, the crest losses were not a primary part of the study. Therefore, the equation developed from the detailed study of crest losses reported in Part XII will be used here to compute the crest energy loss coefficient. This equation is

$$K_c = \left\langle 1 - 2\frac{t_c}{D} \right\rangle^2 + \frac{0.1}{(Z_p/D)^3} + 0.02(B/D)^{5/2} \qquad \text{(XII-9)}$$

where the term in pointed brackets is valid only for $t_c/D < 0.5$ and is zero when $t_c/D \geq 0.5$, t_c is the crest thickness, and Z_p is the antivortex plate height above the crest. The relative crest thicknesses t_c/D were 0.125 for the air model and 0.111 for the water model. The relative antivortex plate height above the crest Z_p/D was 0.5 for all drop inlets. Therefore, the crest loss coefficient K_c as expressed in equation XII-9 became a function only of drop inlet length for each of the two model systems used in this study. The computed coefficients are listed in table XVI-9.

TABLE XVI-9.—*Computed crest energy loss coefficients*

B/D	K_c	
	Air	Water
1.5	1.418	1.460
2	1.476	1.518
3	1.674	1.717
5	2.481	2.523

Though table XVI-9 shows that the crest energy loss coefficient increases with the drop inlet length, the actual head loss for a given discharge decreases as the drop inlet becomes longer. The coefficient increases because as the drop inlet lengthens the velocity head in the drop inlet decreases more rapidly than the crest head loss.

Using equation XII-9, the crest energy loss coefficient K_c has been computed for each series and is listed in table XVI-8.

Barrel Entrance Energy Loss Coefficient

The data presented here shows that the barrel entrance energy loss coefficient is not affected by the Reynolds number or the elbow-transition geometry, but that it is a function of the drop inlet length. The effect of each of these parameters is presented in the following sections.

Effect of the Reynolds number

Figure XVI-19 is a series of plots showing the typical effect of the Reynolds number,

[13] For a theoretical derivation of the crest loss and a comparison with experimental data see Hebaus, G. G., Crest losses for two-way drop inlet. American Society of Civil Engineers Proceedings, Journal of Hydraulics Division, vol. 95, (HY3): 919-940, May 1969.

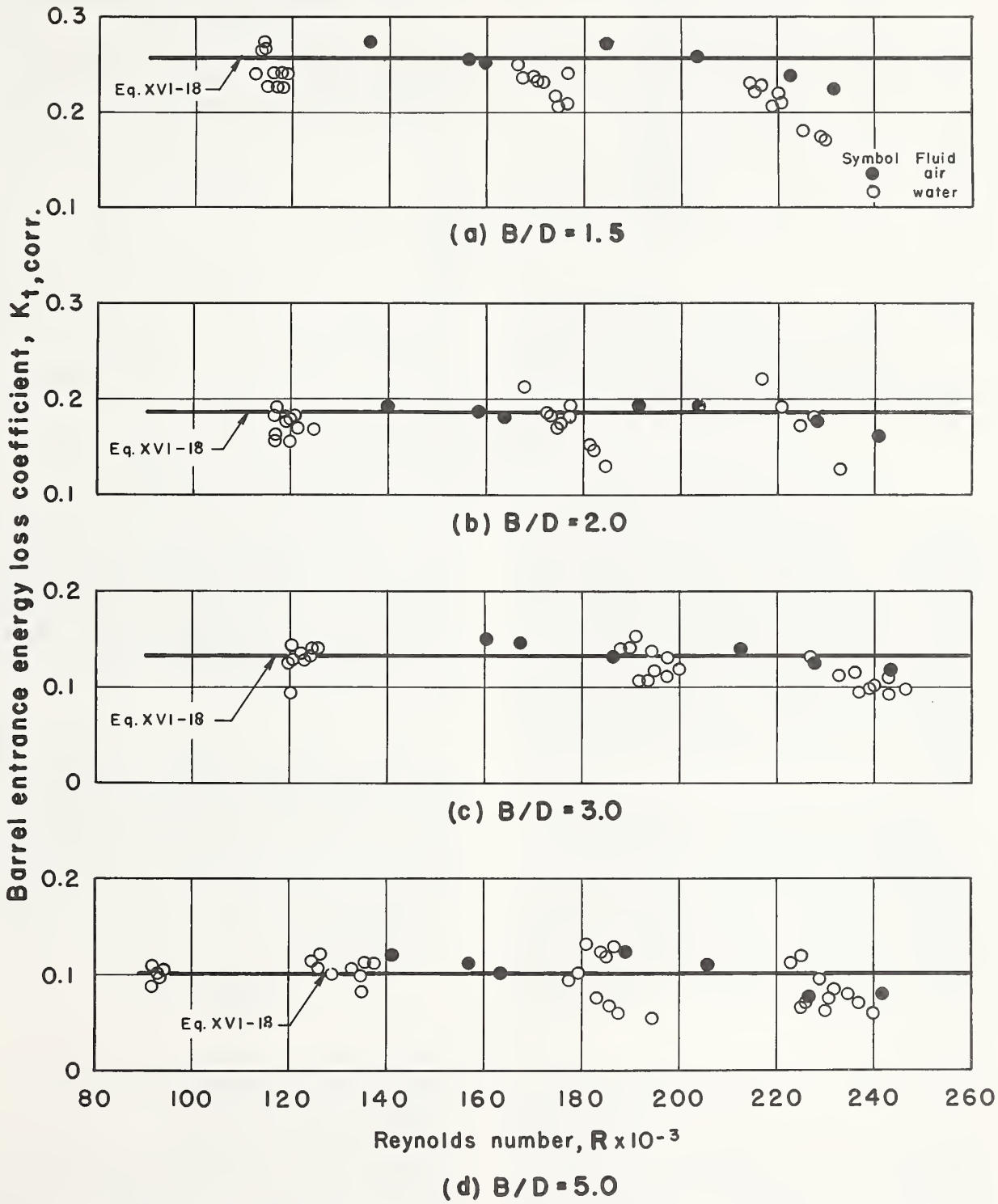

Figure XVI-19.—Effect of the Reynolds number on the barrel entrance energy loss coefficient, $K_{t,corr}$, with elbow 6 and transition F.

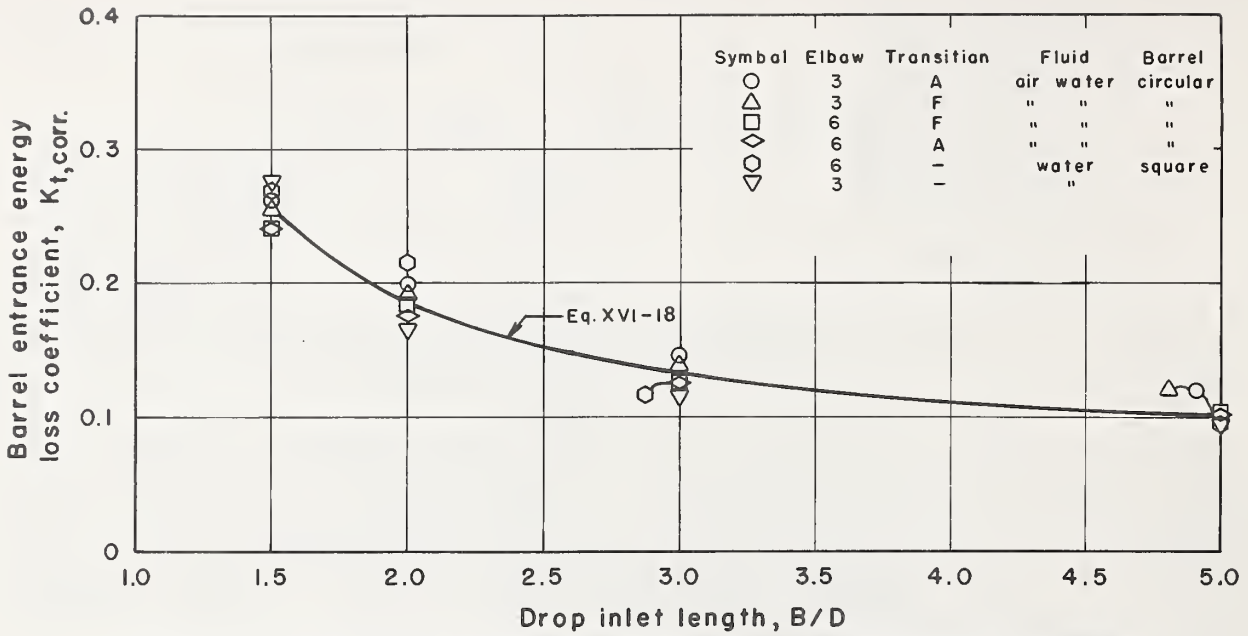

Figure XVI-20.—Barrel entrance energy loss coefficients for several elbow-transition combinations.

$R = V_p D / \nu$, on the barrel entrance energy loss coefficient for each of the four drop inlet lengths tested. These and similar plots of $K_{t,corr}$ for all the air and water tests and all combinations of elbows 3 and 6 and transitions A and F show that the barrel entrance energy loss coefficient is essentially constant for each drop inlet length over the range of the model Reynolds number—approximately 90,000 to 245,000.

The maximum model Reynolds numbers are lower than and only approach the minimum values expected in prototype structures. However, because the barrel entrance energy loss coefficient is shown in figure XVI-19 to be independent of the Reynolds number for $R > 90{,}000$, the barrel entrance energy loss coefficients are assumed applicable to similar prototype barrel entrances with Reynolds numbers greater than 90,000.

Variation with elbow and transition geometry

Figure XVI-20 illustrates the variation with drop inlet length of the barrel entrance energy loss coefficient for combinations of elbows 3 and 6 and transitions A and F. The results are typical of those obtained for all geometries tested. The close groupings of the coefficients for each drop inlet length show that the barrel entrance energy loss coefficients are nearly the same for all elbow and transition combinations used with the circular barrel as well as for the elbows used with the square barrel. This indicates that, for the entrances tested, the barrel entrance energy loss coefficient is independent of the elbow-transition geometry.

Effect of drop inlet length

Figure XVI-20 shows that the drop inlet length has a significant effect on the barrel entrance energy loss coefficient. The reduction in the barrel entrance energy loss coefficient as the drop inlet length increases is the result of a less abrupt change in the flow direction as the drop inlet lengthens.

The equation for the barrel entrance energy loss coefficient is

$$K_t = \frac{0.36}{(B/D)^{1.75}} + 0.08 \qquad \text{(XVI-18)}$$

Equation XVI-18 is plotted in figures XVI-19 and XVI-20 to show its agreement with the data.

Precision of the equation

The computed values of K_t and their differences from the corrected values of the barrel entrance energy loss coefficient are given in table XVI-8. The maximum deviation of the computed K_t from the corrected experimental values is 0.03.

Agreement of the Computed and Observed Entrance Energy Loss Coefficients

The entrance energy loss coefficient K_e is computed by substituting the proper relative cross section area terms into equation XVI-15. For the two-way drop inlet with a circular barrel

$$K_e = K_c\left(\frac{\pi}{4B/D}\right)^2 + K_t \qquad \text{(XVI-19)}$$

and for the two-way drop inlet with a square barrel

$$K_e = K_c\left(\frac{1}{B/D}\right)^2 + K_t \qquad \text{XVI-20)}$$

In these equations the crest loss coefficient K_c is given by equation XII-9 and the barrel entrance loss coefficient K_t is given by equation XVI-18.

Computed values of K_e are listed in table XVI-8 and compared with the observed K_e values for each series. The differences between the computed and the observed entrance loss coefficients vary from -0.04 to 0.03 for the air tests and from -0.02 to 0.09 for the water tests. Observed values of K_e averaged for each drop inlet length and elbow-transition combination are plotted in figure XVI-21. Also shown are curves representing equations XVI-19 and XVI-20. Equations XVI-19 and XVI-20 well represent the observed entrance energy loss coefficients.

The agreement of the computed and the experimental entrance energy loss coefficients is also shown in table XVI-10 as the percentage of tests for which the difference between the computed and experimental values of K_e is equal to or less than specific limits for each drop inlet length. The computed values of K_e differ from the observed values by 0.05 or less for essentially all test conditions, a slightly greater difference occurring with the shortest drop inlet for the water tests.

TABLE XVI-10.—*Percentages of tests for which the differences between the computed and experimental values of K_e were equal to or less than specified limits*

Difference limits	B/D			
	1.5	2	3	5
±0.01	38	43	67	62
± .02	67	81	95	86
± .05	86	100	100	100

Experience has shown that values of K_e agreeing to within 0.05 represents about the limit of precision of the experimental method. Therefore, the agreement shown in tables XVI-8 and XVI-10 and figure XVI-21 is highly satisfactory.

Compatibility Limitations

The compatibility requirement of K_c and K_t between this and other closed conduit studies at the St. Anthony Falls Hydraulic Laboratory was discussed in the section **Barrel Entrance Energy Loss Coefficient Correction.**

Caution must also be used in combining individual loss coefficients from tests made at different laboratories. Unless similar piezometer locations on geometrically similar models were used, the coefficients will not be compatible.

Comparison of Barrel Entrances

A comparison of the entrance energy loss coefficients for various two-way drop inlet barrel entrance geometries illustrates the effectiveness of the elbow and transition in reducing entrance losses. This comparison is made in table XVI-11.

CONCLUSIONS

Of the elbow shapes tested, elliptical elbow 3 had the lowest cavitation potential. Elbow 6 was the best of the double circle elbows tested, but its lower pressure coefficients and steeper adverse pressure gradients show it to be inferior to elbow 3. However, use of elbow 6 will be satisfactory for many situations.

Conical transition A and warped transition F had closely similar pressure coefficients and adverse pressure gradients, transition A being slightly better.

The barrel entrance energy loss coefficients for all combinations of elbows 3 and 6 with transitions A and F are identical and vary only with drop inlet length. The coefficients for elbows 3 and 6 when used with square barrels are also identical, varying only with drop inlet length.

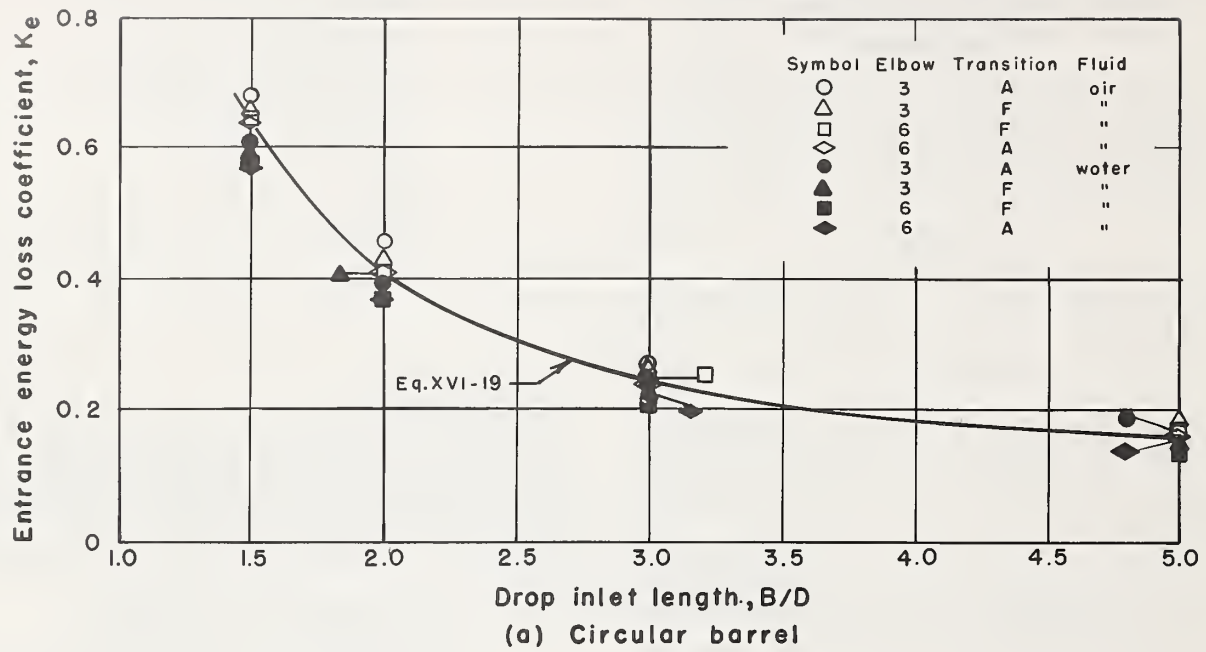

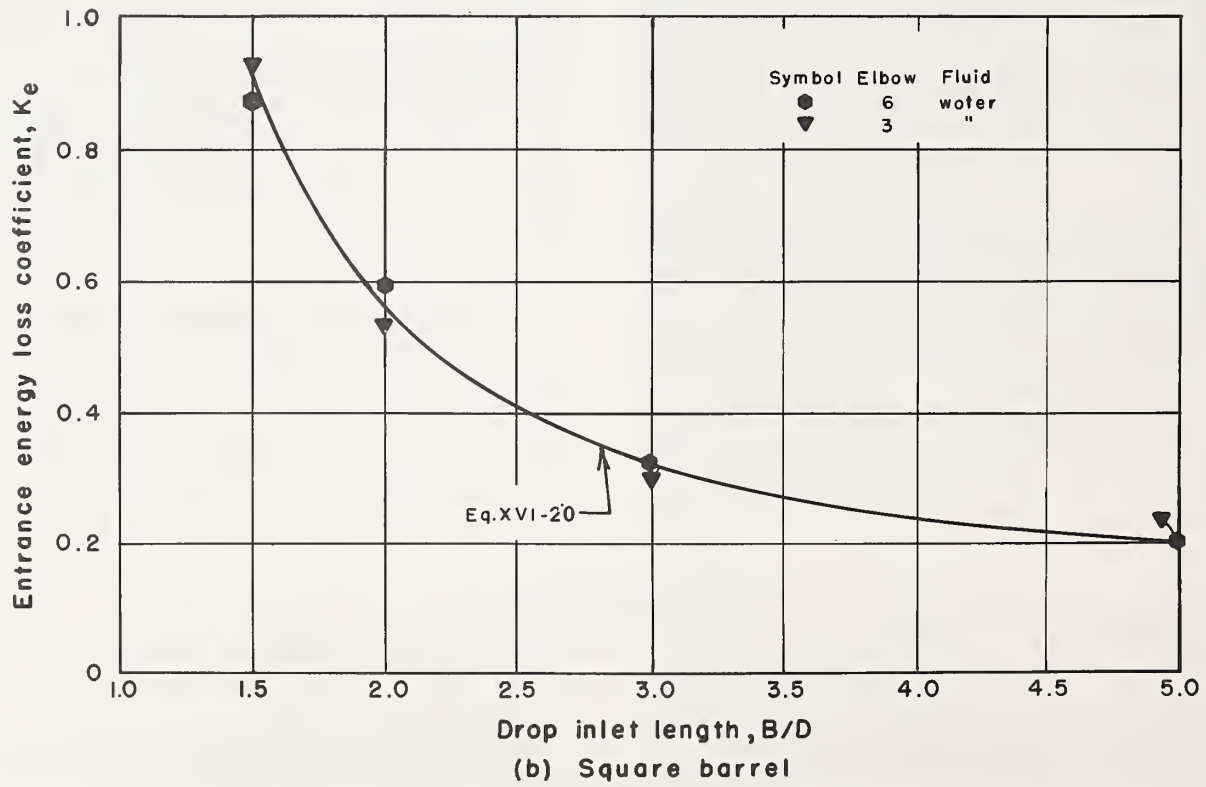

Figure XVI-21.—Entrance energy loss coefficients for elbows 3 and 6 with and without transitions A and F with circular and square barrels. (A) Circular barrel. (B) Square barrel.

SUMMARY

For convenience of use by designers, the elbow and transition shapes, the energy loss coefficients, and the minimum average and average minimum instantaneous pressure coefficients for elbows 3 and 6 and transitions A and F are summarized below.

Elbows

Elbow 3 is a quarter ellipse having the equation

$$\left(\frac{x}{2D}\right)^2 + \left(\frac{y}{D}\right)^2 = 1$$

Elbow 6 is comprised of two circular arcs. The upstream arc has a radius of **D**/2 and an angle of 45°. The following arc has a radius of 3**D**/2 and an angle of up to 45°.

Both elbows are terminated at the point where the slope of the curve equals the barrel slope.

TABLE XVI-11.—*Entrance energy loss coefficients for closed conduit spillways with two-way drop inlets 1D wide and 5D high*

Description of spillway	B/D	K_e
Circular barrel:		
Two-way drop inlet with flat, horizontal invert and square-edged entrance to barrel on zero slope; $t_c/D = 0.125$, $Z_p/D = 0.5$ (Part XII)	5	0.53
	3	.63
	2	.83
	1.5	1.10
Two-way drop inlet with horizontal, semicylindrical invert and square-edged entrance to barrel on zero slope; $t_c/D = 0.125$, $Z_p/D = 0.5$ (Part XVII[1])	5	.53
	3	.63
	2	.83
	1.5	1.10
Two-way drop inlet with horizontal, semicylindrical invert and elbow-transition entrance to barrel on zero slope; $t_c/D = 0.125$, $Z_p/D = 0.5$ (Part XVI)	5	.16
	3	.25
	2	.42
	1.5	.65
Two-way drop inlet with Swarthmore elbow invert and Swarthmore elbow-transition entrance to barrel on zero slope[2]; $t_c/D = 0.375$, $Z_p/D = 0.58$	2	.17 .37
Square barrel:		
Two-way drop inlet with flat, horizontal bottom and a 90° circular elbow entrance to barrel on zero slope[3]	3	.40
Two-way drop inlet with flat, horizontal bottom and elbow entrance to barrel on zero slope; $t_c/D = 0.111$, $Z_p/D = 0.5$ (Part XVI)	5	.20
	3	.32
	2	.57
	1.5	.91

[1] In press.

[2] See footnote 5, page 2.

[3] Payne, A. S., Entrance Head Losses in Drop Inlet Spillways, Design Note No. 8, Engineering Division, Soil Conservation Service, U.S. Department of Agriculture, August 19, 1969.

Transitions

Transition A is 2**D** long, has a semicylindrical invert of **D**/2 radius laid on the barrel slope, plane vertical triangular sides tapering from **D**/2 high at the upstream end to a vertex at the downstream end **D**/2 above the barrel invert, a plane isosceles triangular top having a base **D** wide at the upstream end and its vertex at the downstream end laid on the barrel slope, and oblique quarter cones between the vertical sides and the top. Transition A is shown in figure XVI-3.

Transition F is 1**D** long, has a plane isosceles triangular top with a base of **D** length at the upstream end and laid on the barrel slope, and warped sides between the triangular top and the barrel that are formed by successive lines from the sides of the triangular top normal to the barrel axis and tangent to the barrel circumference. Transition F is shown in figure XVI-4(d).

Energy Losses

Crest loss coefficient, K_c

$$K_c = \left\langle 1 - 2\frac{t_c}{D} \right\rangle^2 + \frac{0.1}{(Z_p/D)^3} + 0.02\left(\frac{B}{D}\right)^{5/2} \qquad \text{(XII-9)}$$

where the term in pointed brackets is zero when $t_c/D \geq 0.5$.

Barrel entrance energy loss coefficient, K_t

$$K_t = \frac{0.36}{(B/D)^{1.75}} + 0.08 \qquad \text{(XVI-18)}$$

Entrance energy loss coefficient, K_e

with circular barrel

$$K_e = K_c\left(\frac{\pi}{4B/D}\right)^2 + K_t \qquad \text{(XVI-19)}$$

with square barrel

$$K_e = K_c\left(\frac{1}{B/D}\right)^2 + K_t \qquad \text{(XVI-20)}$$

Minimum Average Pressure Coefficients

Circular Barrel

elbow 3

$$\frac{h_n}{h_{vp}} = 0.22 \qquad \text{(XVI-2)}$$

elbow 6

$$\frac{h_n}{h_{vp}} = 0.04\left\langle 2.75 - \frac{B}{D} \right\rangle + 0.08 \qquad \text{(XVI-3)}$$

where the term in pointed brackets is zero when $B/D \geq 2.75$

transition A

$$\frac{h_n}{h_{vp}} = \frac{0.14}{(B/D)^{0.3}} - 0.1 \qquad \text{(XVI-4)}$$

transition F

$$\frac{h_n}{h_{vp}} = \frac{0.18}{(B/D)^{1.30}} - 0.1 \qquad \text{(XVI-5)}$$

Square barrel

elbow 3

$$\frac{h_n}{h_{vp}} = -0.01\frac{B}{D} + 0.02 \qquad \text{(XVI-6)}$$

elbow 6

$$\frac{h_n}{h_{vp}} = \frac{0.25}{B/D} - 0.30 \qquad \text{(XVI-7)}$$

Instantaneous Minimum Pressure Coefficients

For a circular barrel add

$$\frac{\Delta h_n}{h_{vp}} = -\frac{0.57}{(B/D)^{1.17}} \qquad \text{(XVI-8)}$$

to the minimum average pressure coefficients for elbows 3 and 6 and transitions A and F.

For a square barrel add

$$\frac{\Delta h_n}{h_{vp}} = -\frac{0.92}{(B/D)^{1.17}} \qquad \text{(XVI-9)}$$

to the minimum average pressure coefficients for elbows 3 and 6 with flat inverts.

NOMENCLATURE

a	a dimensionless parameter in equation XVI-1
A_p	cross-sectional area of barrel
A_r	cross-sectional area of drop inlet
B	drop inlet length
D	barrel diameter and drop inlet width
g	gravitational acceleration
h_c	head loss at drop inlet crest
h_e	total head loss for drop inlet, elbow, and transition
h_n	local pressure head deviation from the friction gradeline
Δh_n	fluctuation of local pressure head
h_t	head loss caused by elbow and transition
h_{vp}	velocity head in barrel
K_c	crest energy loss coefficient
K_e	entrance energy loss coefficient
K_t	barrel entrance energy loss coefficient
$\Delta K_t'$	difference between observed and estimated barrel entrance loss coefficients
K_t'	estimated barrel entrance loss coefficient
n	any point along conduit
Q	discharge
R	Reynolds number $= V_pD/\upsilon$
t_c	crest thickness
V_p	flow velocity in barrel
V_r	flow velocity in drop inlet
x	distance from elbow entrance or beginning of elbow curvature
X	distance from transition entrance
y	distance from barrel crown
Y	distance above transition and barrel centerline
Z_p	antivortex plate height
υ	kinematic viscosity
ϕ	obtuse angle between horizontal and tangent to free streamline
$\langle\ \rangle$	quantity in pointed brackets is zero for negative numbers

GPO 821-975-2

U.S. DEPARTMENT OF AGRICULTURE
SCIENCE AND EDUCATION ADMINISTRATION
NORTH CENTRAL REGION
PIONEER INDUSTRIAL PARK
2000 WEST PIONEER PARKWAY
PEORIA, ILLINOIS 61614

OFFICIAL BUSINESS
PENALTY FOR PRIVATE USE $300

POSTAGE AND FEES PAID
U.S. DEPARTMENT OF
AGRICULTURE
AGR 101

U.S.MAIL

4381

4075 HJELAA203A112 03032 0001
PROF A HJELMFELT
UNIVERSITY OF MISSOURI
2039 ENGINEERING BLDG
COLUMBIA MO 65201